High Performance Propellant Development - Overview of Development Activities Regarding Premixed, Green N_2O/C_2H_6 Monopropellants

Estoril, Portugal / 09 – 13 MAY 2022

Michele Negri(1), Lukas Werling(1) , Felix Lauck(1), Elke Goos(2), Janine Wischek(3), Yasuko Besel(3), Ferran Valencia-Bel(4)

(1) Institute of Space Propulsion, German Aerospace Center (DLR), 74239 Hardthausen, Germany
(2) Institute of Combustion Technology, German Aerospace Center (DLR), 70569 Stuttgart, Germany
(3) Institute of Material Research, German Aerospace Center (DLR), 51147 Cologne, Germany
(4) ESA/ESTEC-Chemical Propulsion, European Space Agency (ESA), 2200 AG Noordwijk, Netherlands

KEYWORDS: Green propellants, nitrous oxide fuel blends, HyNOx, premixed monopropellant, nitrous oxide, ethane, N_2O, C_2H_6, ESA project, material compatibility, thermal stability, combustion tests, propellant mixing

ABSTRACT:

The global search for green alternatives to the highly toxic monopropellant hydrazine (N_2H_4) is still ongoing. Different alternatives for hydrazine with different degrees of maturity are currently under investigation. One of these alternatives are mixtures of nitrous oxide and fuels. These propellants offer a high performance (I_{sp} approx. 300 s), low propellant costs and are non-toxic. In the frame of the ESA activity “High Performance Propellant Development”, DLR investigates a premixed N_2O/C_2H_6 propellant and assesses the safety and performance properties of the mixture.

To study the propellant properties DLR built a liquefaction and mixing setup which allows condensation, pressurization and mixing of liquid N_2O and C_2H_6. The produced propellant mixture was used to feed a thermal stability, a material compatibility as well as a priming/water hammer test setup. Furthermore, the gaseous propellant was used to conduct ignition test under vacuum conditions. A last work package included hot runs with liquefied N_2O/C_2H_6 propellant supplied to a monopropellant like setup from a single tank.

Despite the premixed nature of the propellant, the thermal stability tests showed no decomposition or combustion of the propellant. The compatibility testing of the propellant with metal alloys Al 2219, Ti64, and stainless steels SS 316 and CRES-15-5 showed no degradation of the material or propellant. In addition, the polymers PTFE (Polytetrafluoroethylene), Kalrez and FEP (Fluorinated ethylene propylene) were tested, here only FEP was incompatible with the propellant.

The priming/water hammer tests also showed no decomposition or combustion of the propellant, even for supply pressures of up to 60 bar.

The ignition tests under vacuum conditions showed a reproducible, good ignitability of the propellant in a 22 N research thruster. The mixture was ignitable for mass mixture ratios of ROF=4 to 11 while the mass flow was changed in between 4 g/s and 10 g/s.

The final task was to conducted a series of hot gas combustion tests with an experimental 22 N thruster. The thruster was fed from a tank with liquified, premixed propellant. During 40 test runs, the propellant showed a reliable ignition and combustion behaviour. The mixture ratio of oxidizer to fuel in the test runs was in between 5.4 and 9.9 and showed very low combustion roughness and high combustion efficiencies (up to 96 %).

Due to the positive results of the activity, the next step is the development of higher TRL thrusters and propulsion systems for the N_2O/C_2H_6 propellant.

Symbols and Abbreviations

$A_{orifice}$	Orifice cross-sectional area [m²]
A_t	Nozzle throat area [m²]
c^*	Characteristic exhaust velocity [m/s]
C_d	Discharge Coefficient of restriction
DLR	German Aerospace Center
d_t	Nozzle throat diameter [m]
$di_{Element}$	Inner diameter of test element [mm]
$d_{orifice}$	Orifice diameter [mm]

ESA	European Space Agency
η_{c*}	c* or combustion efficiency (c^*_{exp}/c^*_{theo})
ε	Expansion ratio (A_e/A_t)
HyNOx	Hydrocarbons and Nitrous Oxide
I_{sp}	Specific impulse [s]
$L_{Elemente}$	Length of adiabatic compression test element [m]
$\dot{m}$	Propellant mass flow [kg/s]
MIST	Mixing and liquefaction setup
ROF	Mass mixture ratio (Oxidizer to fuel ratio)
P_{cc}	Combustion chamber pressure [bar]
P_{Init}	Initial Pressure
ΔP	Pressure drop across orifice/restriction
P&ID	Piping and instrumentation diagram
$\rho_{propellant}$	Density of the propellant [kg/m^3]
T_{on}	Flow control valve opening time [ms]
T_{off}	Flow control valve closing time [ms]

1. INTRODUCTION

Since the early days of spaceflight hydrazine (N_2H_4) is used as a monopropellant to power rockets, satellites or probes [1–3]. During the 50s and 60s of the 20th century a large number of different propellants were tested to be used as a monopropellant [2]. Among these propellants, hydrazine proved to be the best choice. N_2H_4 offered a good performance, long term storability, handling with a very low risk of explosions and relatively low costs. These characteristics make hydrazine the commonly used monopropellant to the present day. Additionally, space flight and the operation of satellites are business areas which are strongly focused on reliability. Thus, the development and qualification of new propellants and suitable thrusters is time consuming and generates high costs.

However, during the last decade several things changed. The high toxicity of hydrazine became a growing point of concern. In the EU the so-called REACH (Registration Evaluation Authorization and Restriction of Chemicals)-Regulation [4] came into effect and hydrazine was included in the list of substances of very high concern (SVHC). Thus it becomes more and more likely that the use of hydrazine will be limited or prohibited in future, even though exceptions for the space industry might be given [5].

To compensate a possible prohibition of hydrazine several so-called green propellants are under development or qualification. Among these green alternatives to hydrazine are monopropellants as e.g. ADN-based propellants [6–8], H_2O_2 [9–12] or HAN based propellants [13–15] as well as bipropellants e.g. H_2O_2 and ionic liquids [16–19] or H_2O_2 and fuels [20–22].

1.1. Mixtures of hydrocarbons with nitrous oxide (HyNOx) / nitrous oxide fuels blends (NOFBX)

A class of low cost and high performance propellants are mixtures of nitrous oxide (N_2O) and fuels, also known as nitrous oxide fuel blends [23–25]. Those propellants are no single species monopropellants, but mixtures of the oxidizer (N_2O) and one or more fuels (e.g. C_2H_2, C_2H_4 or C_2H_6). Nitrous oxide/fuel propellants are stored premixed, i.e. monopropellant-like in one tank. In comparison to a classical bipropellant system, only a single tank, feeding line and valve is needed. Thus, these propellants are sometimes called “premixed monopropellants”, offering a monopropellant like system while having a bipropellant performance (I_{sp} up to. 320 s). To simplify the liquefaction of the propellant, the components can be cooled down and mixed. The high vapor pressure of the mixtures (approx. 50 bar at 20°C) offers a self-pressurizing propulsion system without any external pressure supply. Beside the mentioned advantages, nitrous oxide fuel blends provide some non-minor challenges: Very high combustion temperatures (approx. 3000 K) require an active cooling of the nozzle and combustion chamber. Furthermore, the propulsion system needs proper flashback arresters and newly designed ignition and injection systems. If a flame flashback or an unwanted ignition occurs, the flame could propagate into the propellant tank and destroy the entire spacecraft. The most known nitrous oxide fuel blend is NOFBX from Firestar/ISPS [23,24]. Furthermore, DARPA and Boeing worked on a nitrous oxide acetylene propellant mixture. During a test campaign with the propellant mixture called NA-7 several explosions occurred [26,27]. Prior to the activities described in this paper, during an ESA activity also mixtures consisting of nitrous oxide and ethanol were examined [25,28,29].

The German Aerospace Center (DLR) in Lampoldshausen and Stuttgart are working on premixed propellants consisting of dinitrogen monoxide/ethene and dinitrogen monoxide/ethane [30–33]. Up to now, the main research activities were the measurements of ignition delay times and of laminar flame velocities, as well as calculation of thermodynamic data and the development of the

reaction mechanism to describe and model the measurement results and to predict the combustion behaviour over a wide range of conditions [34,35]

These results helped to develop suitable flame arresters [36,37]. Furthermore combustion tests were conducted to analyse the propellant performance and to develop experimental thrusters [31,32].

1.2. Activities in ESA's High Performance Propellant Development Project

In the frame of the ESA activity "High Performance Propellant Development", DLR's research activities were extended to assess the miscibility, thermal stability and material compatibility of liquid N_2O/C_2H_6 mixtures. Furthermore, the stability to stimuli (water hammer/adiabatic compression) of the propellant was assessed and vacuum as well as atmospheric combustion tests with the propellant mixture were conducted. Figure 1 shows the work breakdown structure of the project. The first work package (WP 1000) was dedicated to reporting and management. In the second work package (WP 2000) the propellant requirements, the development plan and a theoretical safety assessment of the chosen N_2O/C_2H_6 propellant was conducted. In the frame of the third work package (WP 3000) the already existing liquefaction setup for N_2O and C_2H_6 at DLR was modified and optimized, the thermal stability and material compatibility setups were built and prepared and the material samples were prepared. Then the material compatibility testing was conducted and the post-immersion analysis took place. The fourth work package (WP 4000) dealt with the stability to stimuli of the premixed N_2O/C_2H_6 propellant. Here an adiabatic compression setup was built, followed by the corresponding adiabatic compression tests. Finally, the propellant miscibility and thermal stability was assessed.

The fifth and final work package (WP 5000) centred around hot gas combustion testing with the premixed propellant. Here vacuum ignition tests as well as hot firing tests with liquid, premixed propellant under ambient conditions were performed.

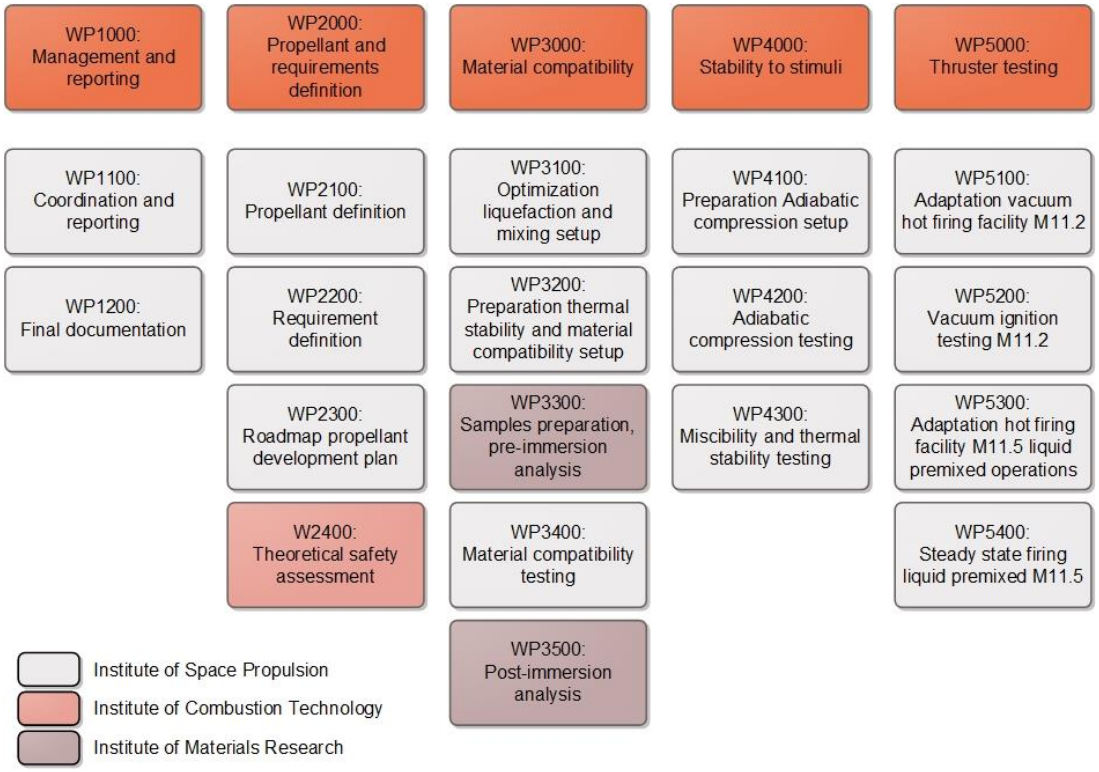

Figure 1: Work Breakdown Structure and Workpackages of the Project

2. WP 2000: Propellant and requirements definition

This work package focussed on the theoretical assessment of the propellant's performance as well as on the theoretical safety assessment.

2.1. Propellant definition

Figure 2 gives the theoretical I_{sp} and the combustion temperature of the N_2O/C_2H_6 propellant depending on the mixture ratio (ROF). The calculations were performed with NASA CEA [38] for a chamber pressure of 10 bar, an expansion ratio of 50 and a frozen flow at the nozzle throat. As Figure 2 shows, for a mass mixture ratio (oxidizer to fuel, ROF) of 7, a maximum theoretical I_{sp} of 301 s is achieved. Thus, the premixed liquefied N_2O/C_2H_6 propellant investigated in the project was aimed to have a mixture ratio of approximately 7. According to mixture data of Refprop [39] the density of the propellant mixture at 39 bar, 273 K and ROF=7 is 728 kg/m^3.

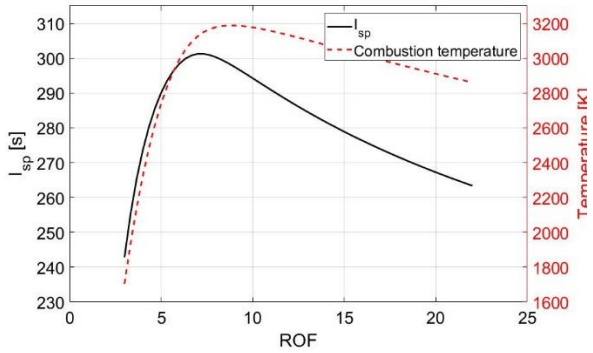

Figure 2: Specific impulse and combustion temperature (epsilon=50, 10 bar, frozen at throat)

2.2. Propellant safety assessment

Chemical and physical properties as well as safety of N_2O and C_2H_6 alone, and their mixtures were assessed theoretically in WP 2400 to be able to give guidelines how to handle safely the propellant mixture and how to prepare safe experimental test environments.

For safe storage and handling of Nitrous Oxide exists effectively an European standard through public available document of European Industrial Gases Association (EIGA) [40]. Also, the Compressed Gas Association (CGA) published and updated regularly at least the following standards for nitrous oxide: CGA G-8.1–2013, Standard for Nitrous Oxide Systems at Customer Sites; CGA G-8.2–2017, Commodity Specification for Nitrous Oxide; CGA G-8.3–2019 Safe Practices for Storage and Handling of Nitrous Oxide.

This information should be considered in design of experimental test environments, e.g. through selection of only compatible materials, and to train people to safely use, handle and store nitrous oxide and its mixtures.

Most relevant chemical and physical properties of pure substances N2O and C2H6 are known in contrast to mixture properties.

For example, NIST Standard Reference Database [39] contains standard fluid thermodynamic and transport properties of single components and the according program REFPROP allows calculation of temperature and pressure depending mixture properties and phase change data as vapor pressure or the calculation of the whole phase diagram under the assumption that selected parameters of equation of state or mixture rule describe the mixing behaviour of the two components well enough.

Some calculation results, as about vapor pressure, will be discussed later in comparison with experimental measurements and tests of WP 4000.

2.3. TNT equivalent calculation

To compare effects, which potential explosive propellant mixtures can have on its surrounding, in comparison to effects, which the well-known explosive 2,4,6-trinitrotoluene (TNT) has, the so called "TNT equivalent" was calculated, which is equating properties of an explosive to TNT.

However, there exist to our knowledge no international agreed definition or norm for the term TNT equivalent or its calculation. As result this term is often misused and misinterpreted, when the property in question and basis for the equivalence is not defined or given [41,42].

Some use TNT equivalent to compare occurring blast waves during explosion or detonation of substances and investigate the resulting craters and structural response of building [41]. Other determine a TNT equivalent by several calculation procedures or more or less defined tests such as the sand crush test or the plate dent test [42]. But these experimental tests and calculations do not necessarily measure the same output property of the same sample substance. For example, the plate dent test is a reasonable measure of Chapman–Jouguet (CJ) pressure, where on the other hand test results of sand crush test do not correlate with Chapman–Jouguet pressure. These results correlate better with the heat energy released by the explosive.

In this project the enthalpy of combustion ΔH_C of a gaseous N_2O/C_2H_6 mixture for a constant-volume

combustion was calculated and divided by enthalpy of combustion ΔH_C of 2,4,6-trinitrotoluene as approximate of the TNT equivalent for gaseous deflagrations, as well as gaseous detonations. Additionally, the Chapman–Jouguet detonation velocity was calculated, too and compared with the detonation velocity of TNT.

The calculations were performed with Gaseq Equilibrium Program Version 0.79 [43] for a gaseous N_2O/C_2H_6 mixture of an equivalence ratio of 1.46 (Mass ratio of oxidizer to fuel (ROF) of 7, corresponding to 4.79452 mol N_2O and 1 mol C_2H_6) and a starting temperature of 300 K and a pressure of 1 atm under adiabatic and constant volume conditions.

State of the art thermodynamic properties were used to calculate the combustion process and the composition of the gaseous combustion products.

For the calculations the following fuel rich gaseous combustion products were considered: nitrogen (N_2), water (H_2O), hydrogen (H_2), hydrogen atoms (H), hydroxyl radical (OH), oxygen atoms (O), carbon dioxide (CO_2), carbon monoxide (CO), cyano radical (CN), hydrogen cyanide (HCN), ammonia (NH_3), methane (CH_4), ethene (C_2H_4), ethyne (acetylene, C_2H_2), methyl radical (CH_3), formaldehyde (CH_2O), formyl radical (HCO), amino radical (NH_2), nitrene (imidogen, NH), nitrogen atoms (N), nitric oxide (NO), methylidyne (hydridocarbon, CH), carbene (CH_2). Additionally, CJ-detonation properties were calculated with the same assumptions and input parameter.

For comparison the defined energy equivalent of TNT given by NIST in its Guide for the Use of the International System of Units (SI) [44] is used. Here the energy equivalent of a ton of TNT as 4.184 E+09 Joule, resulting in an energy equivalent of 4184 kJ/kg TNT, which is equal to 1000 kcal/kg TNT.

In Table 1 the calculation inputs and outputs, as well as the calculated TNT equivalents are shown.

Table 1: Input parameters and calculation of TNT equivalent of HyNOx propellant

Educts, gaseous	4.79452 mol N_2O, 1 mol C_2H_6 (Φ = 1.46, ROF = 7)		
Educts temp.	300 K		
	Adiabatic T & composition at constant V	Adiabatic T & composition at constant V	CJ-detonation with rich products
Educts pressure	1 atm	60 atm	1 atm
Products temperature	3497 K	3979 K	3704 K
Products pressure	21 atm	1373 atm	40 atm
Enthalpy Products in gas. state	590.78 kcal/kg	620.83 kcal/kg	738.60 kcal/kg
Enthalpy Educts in gas. state	307.36 kcal/kg	307.36 kcal/kg	307.36 kcal/kg
Enthalpy difference	283.42 kcal/kg	313.47 kcal/kg	431.24 kcal/kg
TNT-Equivalent	**0.28**	**0.31**	**0.43**
CJ velocity			2298.53 m/s (Ma= 8.386)
Ratio CJ velocity to CJ velocity of TNT			**0.33**
Free Energy Products in gaseous state			9025.02 kcal/kg
Free Energy Educts in gaseous state			-81.31 kcal/kg

3. WP 3000: Material compatibility

WP 3000 centred around material compatibility investigations with the polymers PTFE, FEP and Kalrez as well as with the metals Ti-6Al-4V, SS316, CRES 15-5PH and AA21219-T85.

3.1. Materials and specimens

Materials compatibility testing comprises three phases: pre-immersion inspection, immersion in the propellant, and post-immersion inspection. Materials employed for the material compatibility testing were the three polymeric materials PTFE, FEP and Kalrez® 1050 LF and the four metallic materials Ti-6Al-4V, SS316, CRES 15-5 PH in solution-treated condition, and AA2219-T85. O-rings of the selected polymeric materials were used as test specimens (see Figure 3).

Specimen geometry of the metallic materials was a bar with a length of 40 mm and a width of 5 mm for both the tensile tests and the immersion tests, as shown in Figure 4. The thicknesses of the specimens were 2 mm for SS316 and CRES 15-5 and 3 mm for Ti-6Al-4V and AA2219.

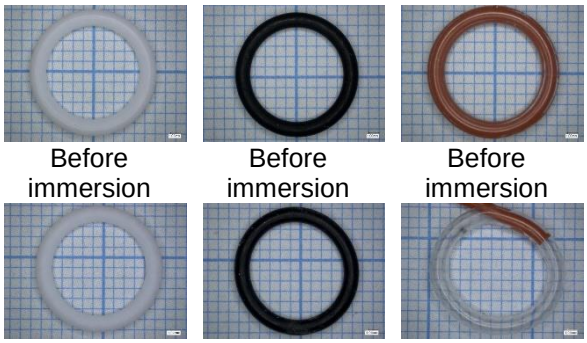

Figure 3 O-ring specimens of polymeric materials

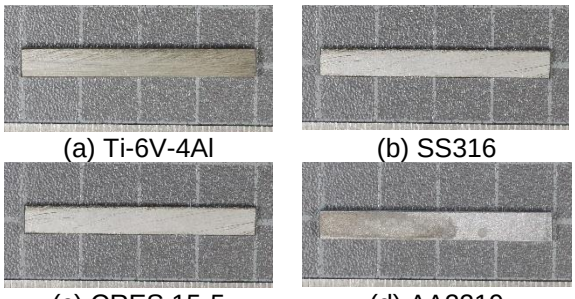

Figure 4 Test specimens of metallic materials after immersion

3.2. Immersion tests

The immersion tests were conducted with a dedicated test setup also used for the thermal stability tests. Every tested material was placed in its own sample container in which the specimens of one material were immersed together. The sample container could be filled via a pneumatically operated ball valve. The sample containers were equipped with a thermocouple and a pressure transducer to measure the internal temperature and pressure. To accelerate aging of the propellant and the metallic samples, the immersion test was conducted at an elevated temperature of 70°C for about 48h. At this temperature the propellant is in supercritical condition. In case of the polymer materials, it was decided to immerse them in the liquid propellant. Therefore, the temperature was set to 30°C and the test duration was 14 days. The specimens were immersed to liquid HyNOx at a ROF around 7 ± 2. In every test run, a container without a material sample was also filled with propellant and exposed to the same conditions as the filled container with the sample to serve as a reference case. The success criteria for the immersion tests were based on changes of the propellant composition. Before and after the immersion tests the propellant was sampled and the ROF and trace gases were determined by means of gas chromatography. The trace gases of interest were nitrogen and carbon dioxide, which could occur when the HyNOx propellant decomposes or reacts. The success criteria in terms of propellant decomposition is based on a maximum decomposition rate of 1 wt% per year for a certain surface (of the specimens) to volume (of the propellant) ratio. For metals a ratio of 1 cm^{-1} is assumed, for polymers 0.1 cm^{-1}. The maximum acceptable decomposition rate is adapted to the shorter test duration at an elevated temperature. The fraction of propellant that is allowed to decompose complies with the ratio of the actual test duration and one year. In addition, for every additional 10 °C above the worst-case maximum storage temperature of 30°C an acceleration of the decomposition by a factor of 2 is considered. This leads to an acceleration factor of 16 in case of the tests with the metallic specimens at 70°C. Consequently, during the material compatibility test with the metallic specimens a fraction of the propellant of 0.08 wt% is allowed to decompose. In case of the polymers a decomposition up to 0.17 wt% of the propellant would be acceptable. The acceptable decomposition rate of the polymers also includes a correction factor because of the different surface to volume ratio between the assumption and the actual configuration of our tests.

Temperature and pressure were monitored during the test duration, but no change related to a possible decomposition of propellant were detected. Further, the gas chromatography

analysis did not detect an increase of the trace gases above the allowed margins. Therefore, it is concluded that the propellant composition did not change due to the contact with the structure of the materials.

3.3. Pre- and post-immersion inspection

Test procedures

To investigate the compatibility of the propellant with the selected materials, tensile tests were conducted on the polymeric and the metallic specimens before and after the immersion tests, respectively. Tensile tests of polymeric materials were performed on the O-rings under displacement control with a displacement rate of 500 mm/min, and tensile strength, elongation at break, and the stress at 100% elongation were evaluated. Five as-received and five immersed O-rings were tested. For the metallic materials, displacement controlled tensile tests were carried out on four specimens each in as-received and immersed conditions with a displacement rate of 1 mm/min. Strain was measured by a laser extensometer with a gage length L_0 of 8 mm. Tensile strength and 0.2% yield strength were evaluated. Due to the specimen geometry without a reduced area, final fracture can occur outside the gage length. Elongation at break was evaluated only when the final fracture occurred within the gage length.

Test results

All FEP O-rings were damaged during the immersion test, while PTFE and Kalrez® O-rings kept their shape after the immersion test, as shown in Figure 3. Therefore, tensile tests were carried out only on PTFE and Kalrez® O-rings.

The tensile test results are shown in Figure 5 and Figure 6. In the diagrams, the error bars indicate the standard deviation. The tensile strength of PTFE O-rings hardly changed, but the value of the stress at 100% elongation were slightly reduced, and the elongation at break was increased significantly by ca. 31%. For Kalrez® O-rings, the tensile strength and the value of the stress at 100% elongation was significantly reduced after immersion. The elongation at break of the immersed Kalrez® O-rings was increased by ca. 13%. As a conclusion of the tensile tests, it is obvious that FEP is not compatible to the

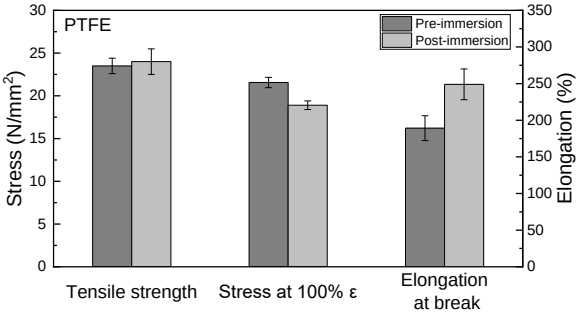

Figure 5: PTFE Tensile test results

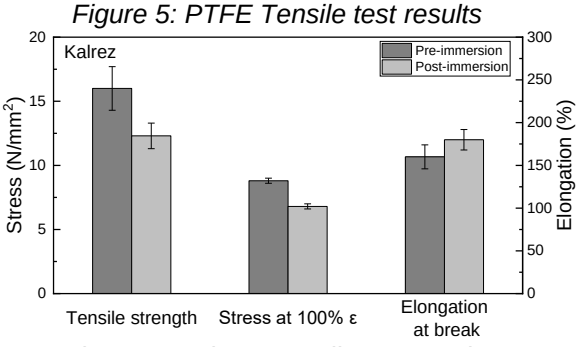

Figure 6: Kalrez® tensile test results

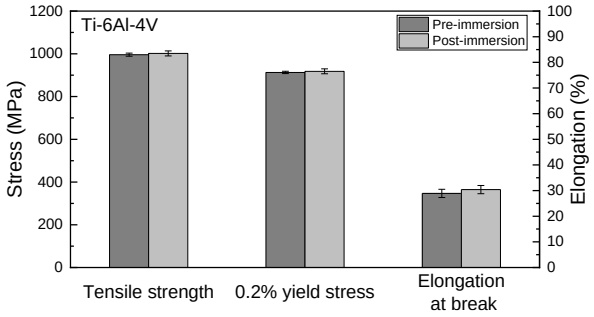

Figure 7: Tensile tests Ti-6Al-4V

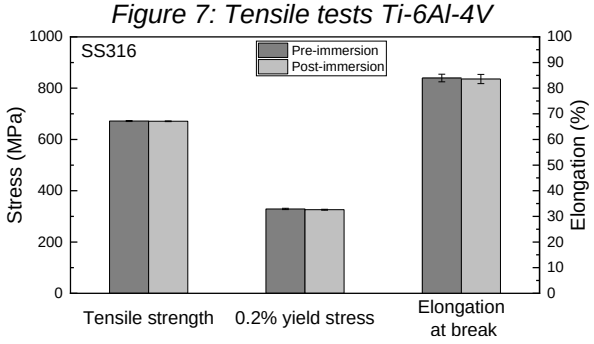

Figure 8: Tensile test SS316

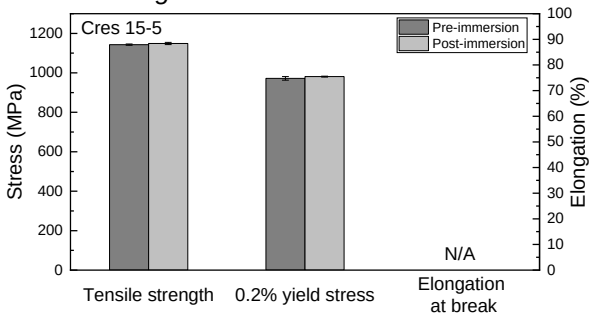

Figure 9: Tensile test Cres 15-5

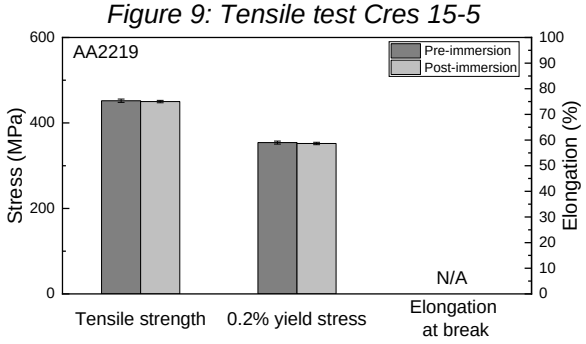

Figure 10: Tensile test AA2219

propellant, and PTFE and Kalrez® are affected in terms of their mechanical properties by being in contact with the propellant, although their O-ring shapes were not changed due to the immersion in the propellant. The tensile test results of the metallic materials are shown in Figure 7, Figure 8, Figure 9 and Figure 10.

The specimens of Cres 15-5 and AA2219 fractured outside of the gage length, and their elongations at break could not be evaluated. As displayed in Figure 7 to Figure 10, the measured mechanical properties of the post-immersion samples were not changed compared to those of the pre-immersion samples. Therefore, it can be concluded that immersion in the propellant has no significant influence on tensile strength, yield stress, and elongation of the selected metallic materials.

4. WP 4000: Stability to stimuli

The fourth work package focussed on the propellant's sensitivity to external stimuli. Here adiabatic compression tests, miscibility investigations and thermal stability test were conducted.

4.1. Adiabatic compression test setup

In the frame of the safety assessment, the behaviour of the liquid premixed propellant in regard to priming and adiabatic compression was investigated. Furthermore, commissioning and reference tests with water and N_2O were conducted. To conduct the investigations a dedicated setup was designed. The setup consists of a test element, a dosing tank, ball valves, connections to the pressurization or vacuum pump and several pressure and temperature sensors. Figure 11 shows a picture of the setup and gives the corresponding piping diagram with the specific elements. The test element (red rectangle) is closed on one side and connected to a ball valve (blue rectangle) on the other side. Two different test elements with a length of 0.75 m and an inner diameter of 4 or 11 mm were used. A dynamic pressure transducer (model 113B23 by PCB piezotronics) with a measurement range up to 690 bar is located at the closed end. The pneumatic operated ball valve is supplied with helium and a small puffer tank was installed close to the valve (marked in green) to allow short opening/closing times. Hence, the valve acts as a fast opening valve (FOV) with a minimum opening time of 12 ms. On the left side (see Figure 11), the valve is connected to the dosing tank highlighted by the orange rectangle, which contains the liquid to be tested. The dosing tank can be closed from two sides and be pressurized with helium or nitrogen. The connection to the vacuum system is only partly visible in Figure 11, as the valve is located in between the orange and blue rectangle. In certain test configurations a needle valve was mounted shortly upstream of the FOV. The needle valve served as an orifice, to restrict the maximum pressure peak. The restriction was intended to protect the setup and measurement equipment from destruction due to the high resulting pressure peaks during the commissioning tests. The most critical condition regarding the priming/adiabatic compression is when the needle valve was removed. In this case the orifice diameter was 4 mm (see Table 2)

For an experimental run, the test element was evacuated. By using the dosing tank, the amount of liquid to be tested is dosed and pressurized to the desired supply pressure. Then the liquid is transferred to the FOV. When the FOV is opened, the resulting pressure peak is recorded by the dynamic pressure sensor (P_{dyn}) at the end of the test element. The data acquisition rate of the dynamic pressure was 100 kHz.

Table 2 shows the test matrix of the conducted adiabatic compression tests. As inert fluids water and nitrous oxide were tested. The test element diameters were varied as well as the orifice diameters. In case of the water tests, the initial pressure was increased in several steps until similar supply pressures as in the N_2O and HyNOx experiments were present. In case of the N_2O and HyNOx the initial pressure was chosen 10 bar above the N_2O vapour pressure at the given ambient temperature.

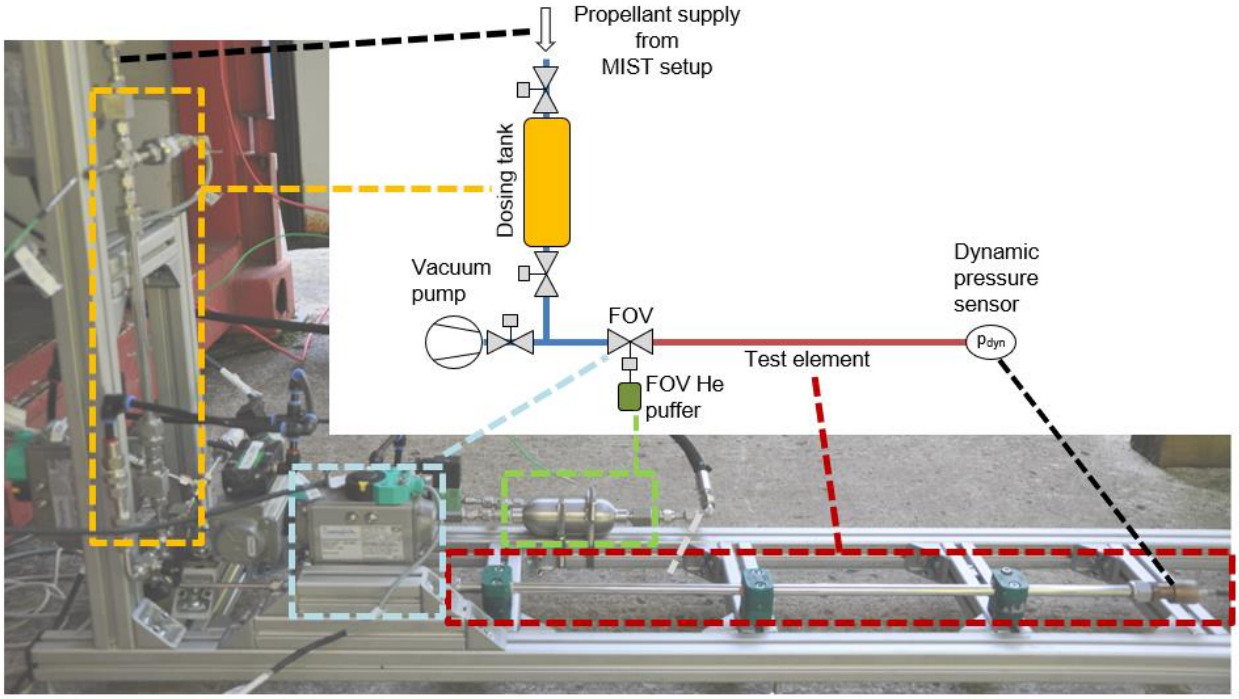

Figure 11: Test setup picture (left and bottom) and corresponding piping and instrumentation diagram (upper right)

4.2. Adiabatic compression test results

Table 2: Test matrix adiabatic compression test

Liquid	$L_{element}$ [m]	$di_{element}$ [mm]	$d_{orifice}$ [mm]	P_{Init} [bar]
H_2O	0.75	4 / 11	1.5 – 4	3 - 60
N_2O	0.75	4 / 11	1.5 – 4	50 - 60
HyNOx (ROF ~7)	0.75	4 / 11	0.5 - 4	50 - 60

Initial tests with water were compared to similar investigation available in literature [45,46]. With the 4 mm test element a demonstration of the water hammer effect was achieved (see red curve in Figure 12). Here, water was pressurized with 20 bar and rushed into the evacuated test element. Further tests with HyNOx show a different behaviour, which can be seen as blue line in Figure 12. At ambient temperatures the HyNOx propellant has a much higher vapor pressure than water. As a result, the pressure peaks observed with water do not occur due to HyNOx' instant evaporation when the FOV is opened. The pressure peaks are damped by the evaporating liquid and this leads to a pressure gradient instead of a sharp pressure peak. All priming experiments conducted with the liquefied N_2O/C_2H_6 propellant and different orifice diameters did not produce any pressure peaks. Moreover, no self-ignition or evidence of a decomposition of the propellant was observed. Therefore, HyNOx is regarded safe in terms of adiabatic compression of the priming operations regarding the presented boundary conditions. However, other critical conditions leading to adiabatic compression such as the fast closure of a valve have not been investigated and the behaviour of the propellant under these conditions is unknown.

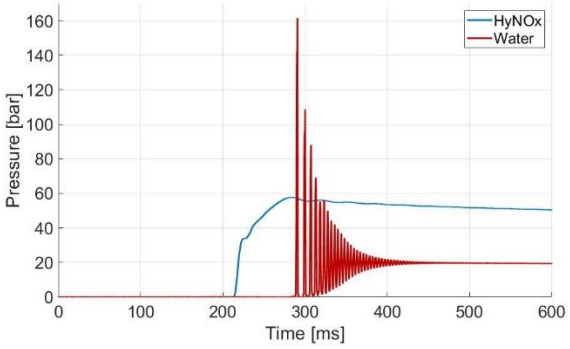

Figure 12 Priming test with water and HyNOx

4.3. Miscibility test setup

To produce the liquid N_2O/C_2H_6 propellant, a specific setup was built and continuously optimized. The setup consists of a N_2O and C_2H_6 gas supply system, fridges to condense N_2O and C_2H_6, a nitrogen or helium supply, transparent metering tubes to adjust the mixture ratio of the resulting propellant, several temperature and pressure sensors and gas sampling ports. The

piping and instrumentation diagram of the setup is shown in Figure 13.

The numbers in Figure 13 correspond to specific step during the propellant preparation procedure. The propellant mixing procedure and the different parts of the mixing setup are described as follows:

1. Evacuation of the whole setup via vacuum pump. Filling of the tanks inside the fridge with gaseous N_2O and C_2H_6. Due to the temperature gradient (ambient temperatures to fridge temperatures) a liquefaction of the two gases takes places.
2. After approximately 60 minutes a transparent polycarbonate tube is filled with N_2O from the cooled tank in the fridge. The polycarbonate-tube is used to pre-dose the N_2O and to adjust the later mixture ratio.
3. Adjustment of the liquid N_2O filling level by using the venting valve $V_{abN2O.}$
4. Filling of the polycarbonate-tube to pre-dose the C_2H_6 according to the wanted mixture ratio.
5. Adjust the liquid C_2H_6 filling level with the venting valve $V_{abC2H6.}$
6. Waiting for the end of boiling of N_2O and C_2H_6 inside the tubes (approx. 5 min). Noting temperature, pressure and filling level of N_2O and C_2H_6. Calculation of the mixture ratio (ROF) via Refprop [39] with the precise data for pressure, temperature and thus density for the liquid and gaseous filling level of the tubes.
7. Mixing of the two fluids via opening of valve V_{Mix}, opening of the connecting gas bridge ($V_{Gas-Mix}$).
8. Waiting for the end of boiling in both connected tubes.
9. Pressurization of the propellant mixture with approximately 60 bar N_2; Waiting period of 30 min to allow condensation of gaseous N_2O and C_2H_6.
10. Transfer of the complete propellant mixture to the tank in the tank section.
11. After waiting additional 30 min, filling of the 3 ml tube section in between V_{Zuend} and V_{Ent} with liquid propellant.
12. Closing of V_{Zuend} and opening of V_{ent} to take a sample of the liquid propellant. Due to the volume change the propellant evaporates into sample container.
13. Venting of gas sample container to 1 bar due to safety reasons, removing gas sample container. Connecting new evacuated gas sample container.
14. Gas chromatography of the samples to analyse the mixture ratio (ROF) and compare it to the calculated values.
15. Repetition of step 11 till 14 to take several samples of the propellant.

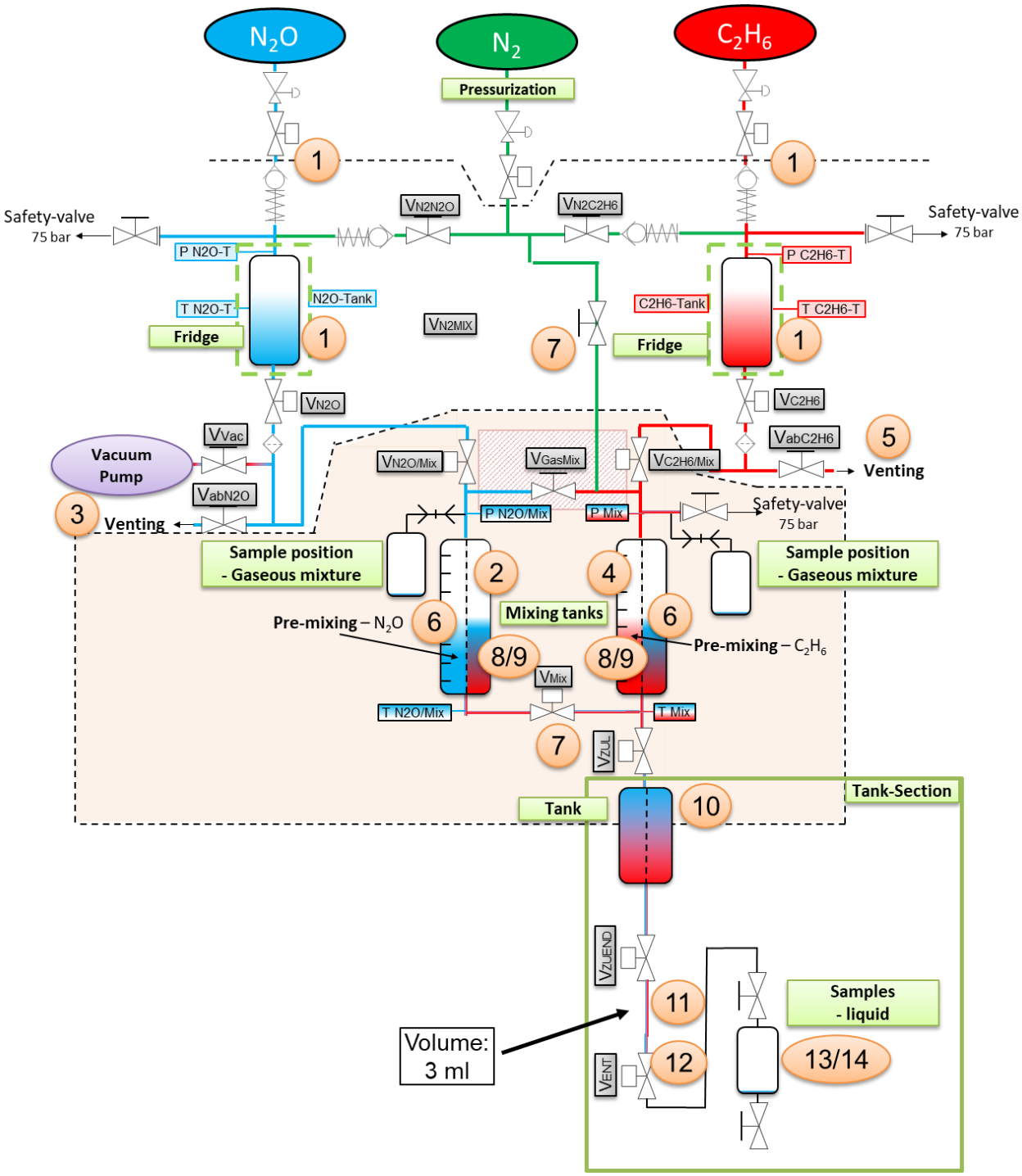

Figure 13: Piping and instrumentation diagram of propellant mixing and sampling setup

4.4. Miscibility test results

The mixing and liquefaction setup (MIST) was used to produce all needed propellant mixtures for the different test activities (adiabatic compression, material compatibility, thermal stability and hot firing). The setup was built and first propellant mixtures were produced. Based on results of the gas samples and the setup's behaviour, several modifications and improvements took place. During this iterative building, testing, sampling, improving cycle of the setup in sum 28 different N_2O/C_2H_6 mixtures were produced. The mixing setup was modified 8 times, up to the point where thy HyNOx composition was reproducible and predictable. The final version of the setup is shown in Figure 13 and made a reproducible production of the propellant at the desired mixture ratio possible. To assess the propellant composition, the setup allowed sampling of liquid and gaseous propellant at different positions. Overall 53 propellant samples were analysed via gas chromatography (gas chromatograph Clarus 580 Perkin Elmer) at DLR's

chemical propellant technology department. The global propellant mass mixture ratios (ROF) after mixing the propellant lay in between 1.5 and 8.3. During all tests no phase separation of the liquified, mixed gases was visible. Via N_2 pressurization with more than 10 bar above N_2O vapor pressure at the current temperature, nearly all gaseous N_2O and C_2H_6 condensates. This condensation process was confirmed by gas sampling of the gas phase. These gas samples showed that - depending on the elapsed time allowing condensation - in between 77% and 98% of the gas phase consisted of N_2.

The liquid propellant samples taken one after each other (with N_2 pressurization) from the 3 ml mixing volume (see Figure 13) showed no mixture ratio shift in between each sample. Furthermore, the mixture ratio (ROF) of the liquid propellant stayed constant at ROF=6.7 for at least 68 h when 3 samples were taken after 1 h, 2 h and 68 h. As result of this investigation, it is assumed that a stable solution of N_2O and C_2H_6 is formed.

In addition, the vapor pressure of the propellant mixture in the tubes after mixing is slightly higher than the vapor pressure of pure N_2O (N_2O has a higher vapor pressure than C_2H_6). This additionally indicates that the liquids form a stable solution. Figure 14 shows two different propellant mixtures, one in the transparent tubes of the mixing setup and the second in the thermal stability test setup.

Table 3 shows an overview of the produced and analysed propellant mixtures during the iterative improvement process of the setup. Initially the setup allowed only gaseous sampling, while later on the propellant could be sampled directly from the liquid phase in the mixing tank (see Figure 13). To analyse if a mixture ratio shift during the sampling process occurs, always more than one sample was analysed.

Table 3: Produced and analysed propellant mixtures

Mixture No.	Number of gas samples analysed	Number of liquid samples analysed
3	6	0
4	6	0
5	4	3
6	4	3
7	2	6
8	2	6
9	0	0
10	0	5
11	0	6
	∑=24	∑=29

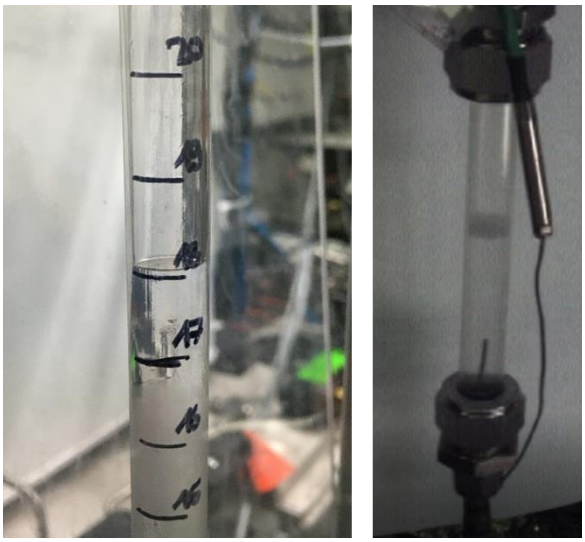

Figure 14: Liquid propellant in mixing setup (left) and liquid propellant in test tube of thermal stability setup to determine vapor pressure (right)

4.5. Thermal stability test setup

Initial tests were conducted to investigate the thermal stability of the HyNOx propellant. The test series is geared to the test 3(c) in the UN "recommendations on the transport of dangerous goods" [47]. This test is "used to measure the stability of the substance when subjected to elevated thermal conditions to determine if the substance is too dangerous to transport." In the original test, 50 g of the substance of interest is placed inside a lipless beaker and closed with a stopper. A known inert reference is placed in a similar second container. Thermocouples are placed inside the sample and reference container, as well as on the outside. Both containers are placed in an electric oven and heated up to 75 °C for 48 hours. Then the temperature is recorded. The test considered as failed if an ignition or explosion occurs or if a temperature difference (i.e. self-heating) of 3 °C or greater is recorded. The thermal stability test is suitable for liquid or solid samples but needed to be adapted to HyNOx as the N_2O/C_2H_6 propellant is a liquefied gas under pressure. The tests were performed with HyNOx at a ratio of oxidizer to fuel (ROF) of around 7. Test temperature and duration were similar to the original UN test 3(c). At these conditions our propellant is expected to be supercritical. Pure ethane and pure nitrous oxide were taken as reference materials.

The thermal stability set up consisted of two containers: one for the propellant (test tube) and one for the reference. In Figure 15 the piping and instrumentation diagram (P&ID) of the thermal stability setup is shown. Both containers were equipped with a thermocouple type K, a 200 bar

STS TM pressure transducer and a pressure relieve valve for safety reasons. The sample containers were placed inside a water bath and the water bath can be set to a certain temperature using a thermostat. The containers could be filled via ball valve, while the overall inner volume of the containers is 18.4 ml. For the tests a HyNOx mixture with an ROF close to 7 was produced with the MIST setup. 10 ml of HyNOx were dosed into the test container using helium as pressurization medium. The tests were conducted for 45 h at an elevated temperature of 75 °C. During the tests pressure and temperature inside the containers were monitored. Further the propellant composition was analysed before and after the test using gas chromatography.

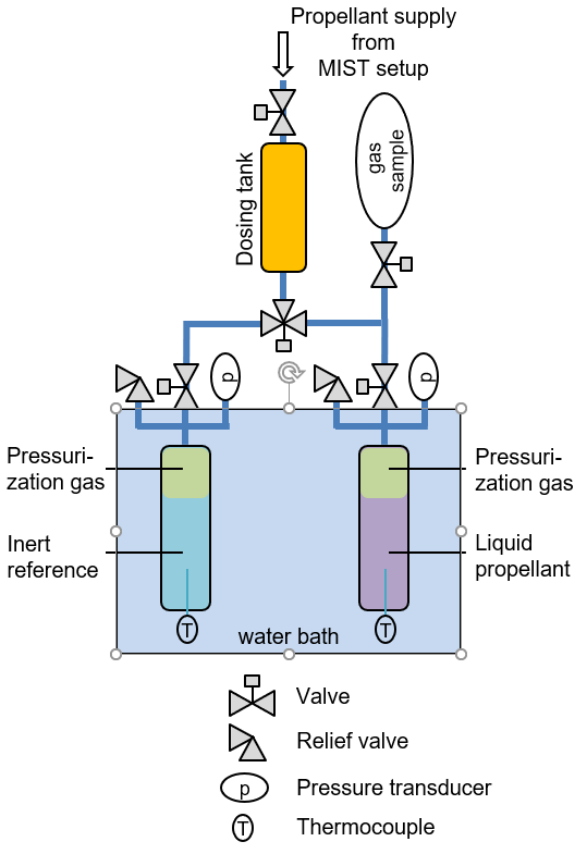

Figure 15 P&ID diagram thermal stability setup

The success criteria in terms of the propellant composition was defined on a maximum acceptable decomposition rate of 1 wt% per year at normal ambient temperature. Further, it was assumed that the elevated temperature accelerates the aging of the propellant by a factor of two for every additional 10°C. Starting from a worst-case temperature of 30°C, the aging in the thermal stability test is accelerated by the factor of 22.6. Hence, in our test conditions the propellant would declared failed if more than 0.12 wt% decompose.

4.6. Thermal stability test results and vapor pressure

Figure 16 shows the recorded pressure data plotted over the corresponding temperature inside the container filled with HyNOx. The red curve indicates the heating process, the black curve indicates the measurement data during the time at the elevated temperature and the blue curve corresponds to the cooling at the end of the test run. During the heating, the propellant's pressure increases from 63 bar at ambient temperature up to 135 bar at 75°C. It can be assumed that the whole sample container is exposed to the water in the bath during the heating process, which results in an evenly distributed, slowly rising temperature in the container. As Figure 16 shows, at the elevated temperature level, the pressure is slowly decreasing. This is related to a small leak of the setup and also a decreasing water level in the water bath. The water bath was refilled several times during the test and thus the pressure loss was partly recovered. At the end of the test the water bath was emptied and the sample container cooled down. It must be mentioned, that with this cooling procedure the temperature decreases faster compared to the heating period and it cannot be assumed the container has the same temperature at every position. This explains, why the pressure at the low temperature is higher than the initial pressure during the heating.

During the tests, no explosion or increase in temperature and pressure of the propellant or the reference substances were observed. Also, the composition of the propellant did not change more than the acceptable margins. Therefore, HyNOx passed the thermal stability test.

In addition, by using the described setup (Figure 15), the vapor pressure at different temperatures was determined. To conduct the vapor pressure determination, a certain amount of HyNOx was filled into the test tube. For these tests, the N_2O/C_2H_6 propellant was not externally pressurized to achieve an equilibrium between the gas and liquid phase. The filling process and existence of both liquid and gaseous phases was confirmed using a transparent tube (see Figure 14 right picture). Unfortunately, this tube could not be used for tests at elevated temperature, because the transparent polycarbonate tube was not able to withstand the pressure at the elevated temperatures. So, for the presented tests regarding the vapor pressure determination, a stainless-steel tube was used and immersed into the water bath to set to a certain temperature. The filling process was conducted simultaneously to the pre-test with the transparent tube.

In Figure 17 the determined vapor pressured for HyNOx at an ROF of 7.2 between 9°C and 42 °C are shown (green circles). The experimental data of Corvaro et al. [48] at lower temperatures and ROF=7 are drawn as red squares. The red triangles mark the data of Corvaro et al. for the conditions where all their liquid mixture was evaporated (in their paper indicated as "superheated vapor"). A power law fit for our experimental measurements and the liquid/gas experimental data of Corvaro is indicted as green, dotted line. Furthermore, the vapor pressure of a N_2O/C_2H_6 mixture at ROF=7 calculated via Refprop [39] is shown (yellow dotted line). Refprop uses a mixture model according to Kunz and Wagner [49].

Both, the calculated vapor pressure via Refprop (yellow dotted line) and the Power law fit of the experimental data (green, dotted line) agree quite well, with maximum deviations of 4 bar at 265 K.

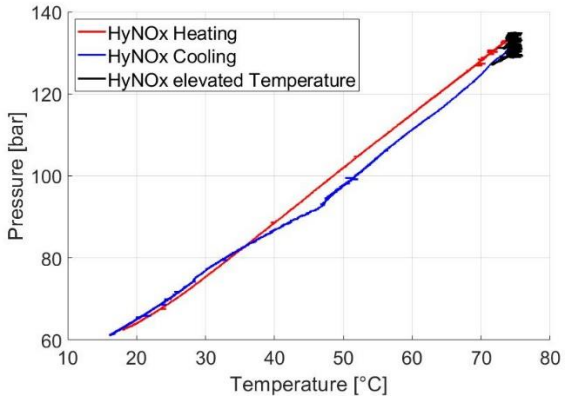

Figure 16: Temperature-pressure diagram during heating of HyNOx-propellant

These deviations could be caused by different test setups, the fitting process and slightly different ROF values. Moreover, the resulting vapor pressure is higher than the individual vapor pressure of the pure fluids at certain temperatures. This means, the actual vapor pressure of HyNOx has a positive deviation from the vapor pressures calculated according to Raoult's law [50].

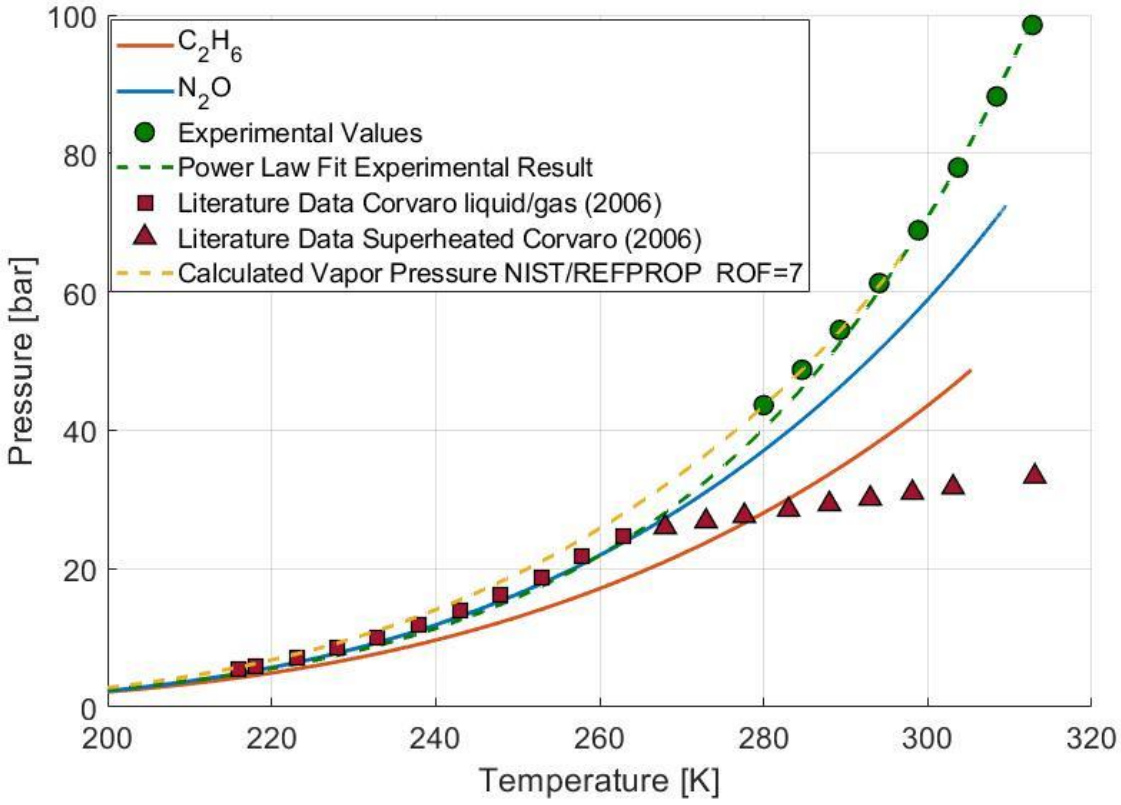

Figure 17: Vapor Pressure of N_2O, C_2H_6 and the propellant mixture at ROF=7.2 compared to literature data of N_2O/C_2H_6 mixtures at ROF=7 [48] and NIST/REFPROP [39] calculations with ROF=7

5. Thruster Testing

This section describes the combustion tests with the premixed HyNOX propellant by using a research thruster. The experiments were conducted under vacuum and atmospheric conditions at different test benches of DLR's M11 test facility [51,52]. *Figure 18* shows the used research thruster with the main parts and the instrumentation. The thruster's design point is 22 N at a mass flow of 7.5 g/s and a mixture ratio (ROF) of 7.

As shown in *Figure 18*, the propellant feeding line is connected to a porous injector which also acts as a flame barrier [36,37,53]. Via two thermocouples the propellant inlet temperature is monitored. Furthermore, the combustion chamber is equipped with thermocouples at different axial positions and a pressure sensor. Combustion of the propellant is initiated via automotive glow plug. At the end of the combustor a nozzle section for atmospheric tests is mounted. In addition, the thruster comprises a regenerative cooling system which was disconnected for the vacuum and hot fire tests during the described activities.

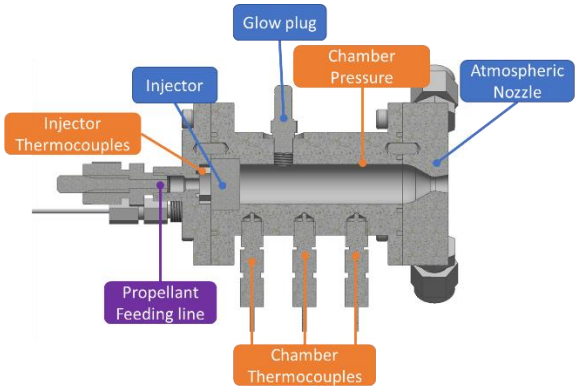

Figure 18: Research thruster with instrumentation

5.1. Vacuum ignition test setup

Figure 19 show the simplified piping and instrumentation diagram (P&ID) of the vacuum test setup. Gaseous nitrous oxide, ethane and nitrogen were fed from the test bench's supply system. The mass flow and mixture ratio of N_2O and C_2H_6 was set by pressure regulators and control valves in the feeding lines of the test bench. The mass flow measurement was performed by two Coriolis mass flow meters in the corresponding feeding lines. Approximately 0.3 m upstream the injector both gases were mixed in a tube cross section. So, in this setup the gaseous propellant was premixed just upstream the injection system. Via nitrogen supply the feeding lines and thruster could be purged before and after the test runs. In parallel to the mass flow measurement (MF-N2O, MF-C2H6), the propellant feeding pressure (P-PROP-IN) and temperature (T-PROP-IN) as well as the temperatures of the propellant at the injector head (T-INJ-01, T-INJ-02) were measured. As shown in *Figure 18*, the chamber pressure and temperatures were recorded as well. The thruster setup was mounted inside the vacuum test bench M11.2 [52]. Before each ignition test, the chamber was evacuated via vacuum pumps to reach a pressure below 10 mbar. The test sequence started with a 10 s preheating of the glow plug, then the N_2O and C_2H_6 main valves were opened and kept open for 6 s. In parallel to the data acquisition, two video cameras were used to monitor the thruster operation (see Figure 22) through windows of the vacuum chamber.

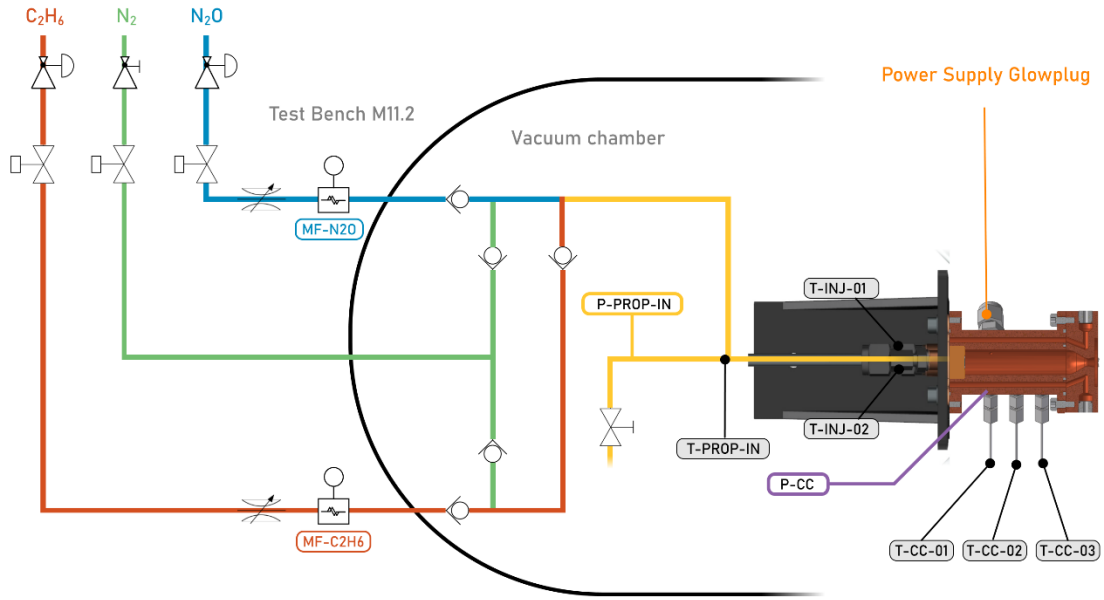

Figure 19: Simplified P&ID of the used test setup for vacuum tests

5.2. Vacuum ignition test results

Overall 33 successful ignition tests of the premixed gaseous HyNOx propellant under vacuum conditions were performed. During the tests the mass flow was varied in between 4.5 g/s and 9.2 g/s, with mixture ratios (ROF) in between 4 and 15. *Figure 20* shows typical test data, in the upper diagram the propellant inlet pressure (red) and the chamber pressure (blue) is shown. The rise time to 90% of the chamber pressure was up to 700 ms due to the length of the tubing in between the valve and the thruster (approx. 2 m). Ignition took place when a chamber pressure in between 1.4 and 1.8 bar was reached.

The lower diagram in *Figure 20* shows the ambient pressure inside the vacuum chamber during the test run. In this case the pressure at ignition was 3 mbar.

Figure 21 shows successful (red squares) and unsuccessful (blue squares) vacuum ignitions depending on mixture ratio and mass flow. The propellant shows a good ignitability in a wide range of mass flows and mixture ratios. The lower limit for ignition regarding the mixture ratio was 4, while below a mixture ratio of 5 the thruster showed a strong combustion roughness and, in some cases, a flame out.

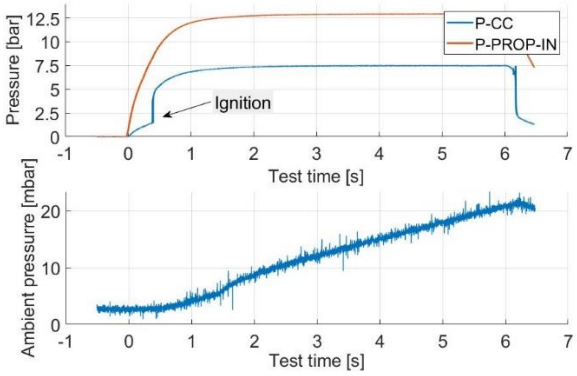

Figure 20: Feeding pressure and chamber pressure (top) and ambient pressure inside the vacuum chamber (bottom)

Thus, for a stable thruster operation it is recommended to stay above ROF=5. To assure a proper ignition, the mass flow of the unburnt gas should be selected such that the needed 1.4 bar chamber pressure is achieved. In our case that resulted in a minimum mass flow of approximately 4.5 g/s.

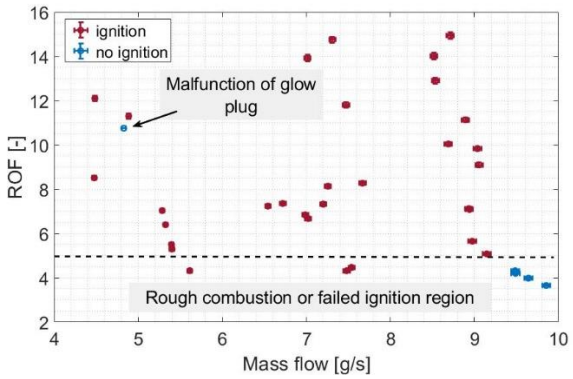

Figure 21: Successful and unsuccessful vacuum ignitions depending on mass flow and mixture ratio

An image of the thruster operating under vacuum conditions is given in Figure 22. As the thruster's nozzle was designed for atmospheric operation, the strong expansion of the exhaust downstream the nozzle can clearly be seen.

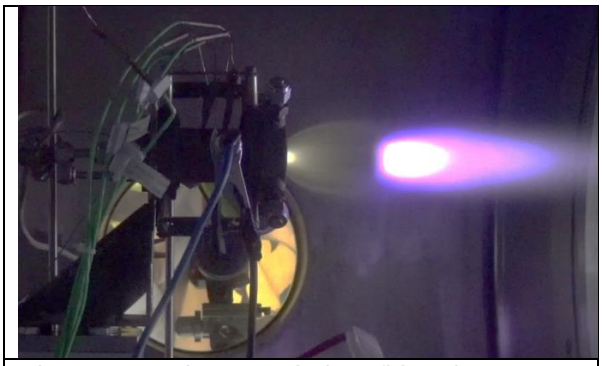

Figure 22: Thruster during firing in vacuum chamber

5.3. Atmospheric hot firing test setup

Subsequent to the vacuum ignition tests, atmospheric tests were conducted. The atmospheric hot firings were performed with premixed propellant fed from one single tank. By using one tank, a typical monopropellant propulsion system should be simulated and steady state firings as well as pulse mode firings in blow down operation were conducted. The piping and instrumentation diagram of the hot firing setup is shown in *Figure 23*. Prior to fuelling, the setup was evacuated up to V_FCV. Following the evacuation, the 150 ml propellant run tank was fuelled by the mixing setup (see Figure 13) using V_Fill. For each test series 100-150 ml of liquid propellant with different mixture ratios (see Table 3) were produced. The propellant condition was monitored via temperature and pressure sensors (T_{Tank} and P_{Tank}). During the hot runs the thruster was fed with propellant vapor taken from the upper part of the run tank (see *Figure 23*). The mass flow into the thruster was calculated by the measurement of the pressure drop across a calibrated orifice ($P_{pre\ orifice}$, $P_{post\ orifice}$). To derive the propellant density, the temperature of the propellant upstream the orifice ($T_{orifice}$) was measured as well. Furthermore, the thruster feeding pressure (P_{feed}), the injection temperature (T_{inject}), the thruster wall temperature (T_{cc}) and the chamber pressure (P_{cc}) were recorded. A connection to the test bench's nitrogen supply allowed purging of the thruster prior and after each test run. The thruster was operated in blow down mode from the run tank. Steady state firings and pulse mode firings with different pulse lengths were performed (see Table 4). To assure a proper ignition, the glow plug was activated 10 s in advance to opening the FCV. During most of the steady state operations, the glow plug was deactivated 1 s after opening of the FCV and ignition of the propellant. For the pulse mode tests, the glow plug was kept activated during the whole test sequence.

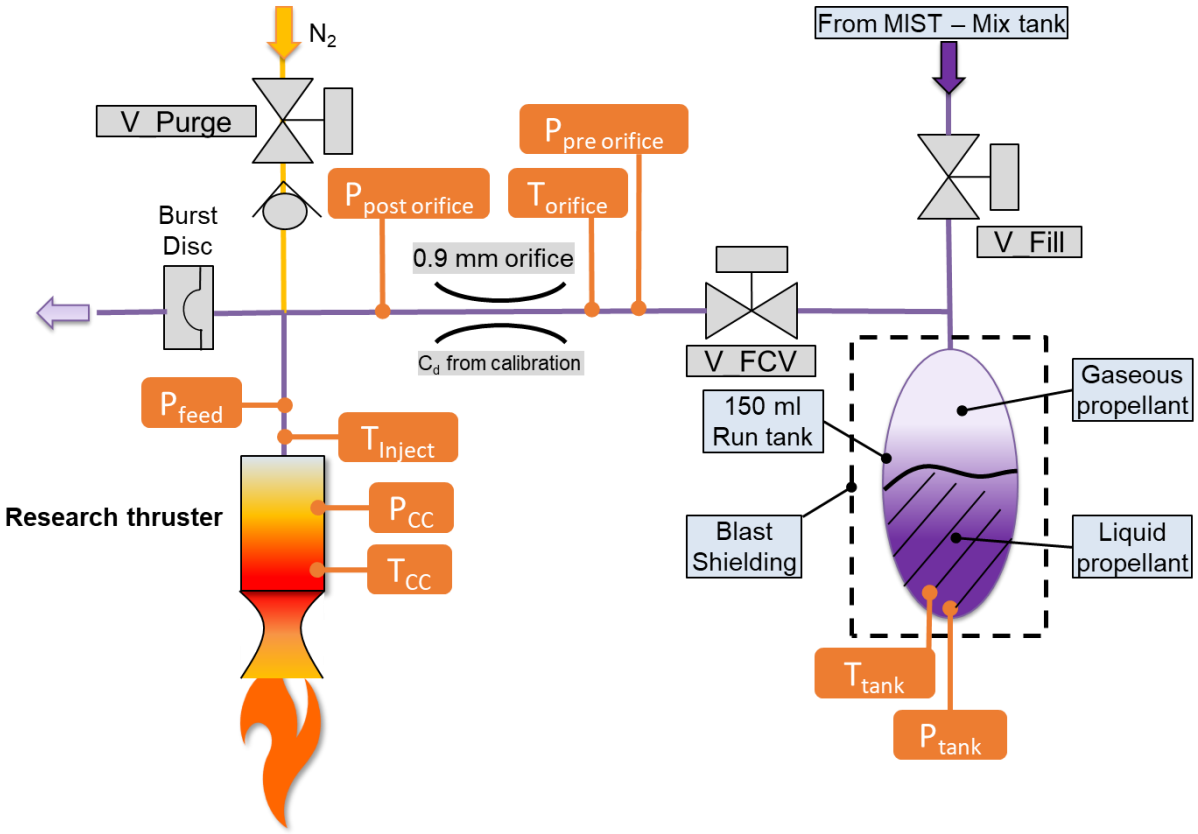

Figure 23: P&ID of hot firing test setup

5.4. Hot firing test results: steady state and pulse mode

Table 4 gives an overview of the conducted tests with the t_{on} and t_{off} times, the number of pulses, the initial liquid ROF of the propellant and the number of test firings. In sum 40 pulse mode and steady state firings were performed while the mixture ratio of liquid propellant was in between 5.4 and 9.9.

Table 4: Overview of conducted hot firing tests under atmospheric conditions

t_{on} [ms]	t_{off} [ms]	Pulses	Initial Liquid ROF	No. of Tests
1.000	0	1	7.1	1
5.000	0	1	7.1	3
20.000	0	1	7.4	1
10.000	0	1	7.4	5
1.000	1.000	10/1	7.3	2
100	900	10	7.3	1
500	500	10	7.3	1
750	250	10	7.3	1
500	500	10	7.5	2
250	750	10	7.5	2
100	900	10	7.5	2
50	950	10	7.5	1
20.000	0	1	7.5	1
10.000	0	1	7.5	1
10.000	0	1	6.5	4
10.000	0	1	9.9	4
10.000	0	1	5.4	4
10.000	0	1	7.7	1
10.000	0	1	6.8	1
500	500	10	6.8	1
250	750	10	6.8	1
				∑ 40 tests

Figure 24 shows the pressure at the tank, the feeding line and inside the combustor during a typical 10 s steady state hot firing in blow down mode. Due to the small run tank (150 ml), the resulting low amount of propellant and the cooling of the run tank caused by evaporation of the

propellant, a significant pressure decay is visible during the run time. Figure 24 shows the first test with a fully fuelled propellant tank, here the over-pressurization with He and the propellants' evaporation delay is visible [54–56]. The evaporation delay describes a phenomenon where the propellant initially starts to boil at the liquid surface only. If now larger quantities of propellant are drained and a further pressure drop above the liquid surface occurs, the whole liquid propellant volume starts boiling. The intensified boiling process results in a slower pressure drop inside the observed volume.

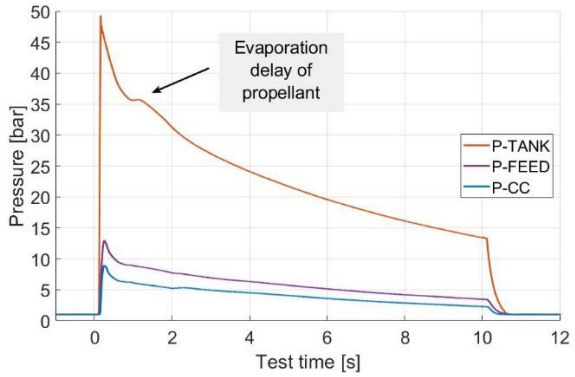

Figure 24: Pressure data during 10 s blow down operation of thruster (liquid propellant ROF=6.8)

As Figure 24 also shows, during the combustion process no strong peaks or oscillations in the chamber pressure are visible. This is caused by the gaseous, premixed state of the propellant mixture as no oscillations are caused by evaporation or mixing processes. The analysis of the chamber pressure shows a combustion roughness lower than 2%.

Figure 25 shows the corresponding mass flow to the pressure data shown in Figure 24. The mass flow is calculated via equation (1) and the density for the corresponding temperature and pressure is obtained via Refprop database [39]. If now the propellant is still pressurized with N_2 or He above the current vapor pressure, Refprop calculates the density values for the liquid propellant as it is assumed that under the higher pressures a liquid mixture flows through the orifice. In reality, of course, initially only N_2 or He with probably some droplets of propellant mixture pass the orifice. Thus, initially the mass flow values in *Figure 25* show a peak and most likely the shown mass flow during the first 1-2 seconds is not correct.

$$\dot{m} = C_d \cdot A_{Orifice} \cdot \sqrt{2\rho_{propellant} \cdot \Delta p} \qquad (1)$$

Figure 26 gives the calculated c* values for the test run shown in *Figure 25* and Figure 24, c* was calculated according to equation (2):

$$c^* = \frac{P_{cc} \cdot A_t}{\dot{m}} \qquad (2)$$

Due to the faulty calculation of the mass flow during the first two seconds of the hot run, the initial c* shows large fluctuations (see *Figure 26*). Thus, the average c* was evaluated in between t=2 s to t=10 s as marked in *Figure 26*. The average c* and η_{c^*} values for the conducted test runs with different mixture ratios can be found in Table 6.

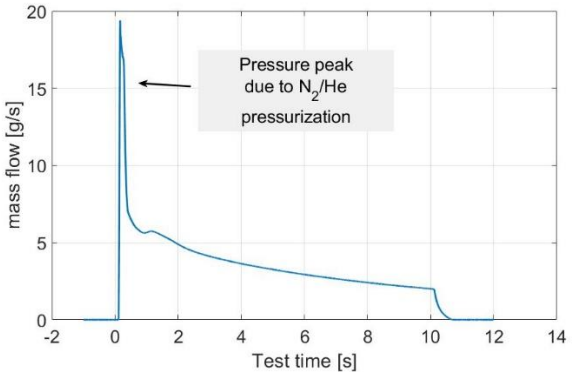

Figure 25: Propellant mass flow during 10 s blow down operation (liquid propellant ROF=6.8)

The average c* for the test shown in *Figure 26* is 1578 m/s which results in a combustion efficiency $\eta_{c^*}$of 95.6 %.

Figure 29 shows a picture of the thruster during a 10s hot firing.

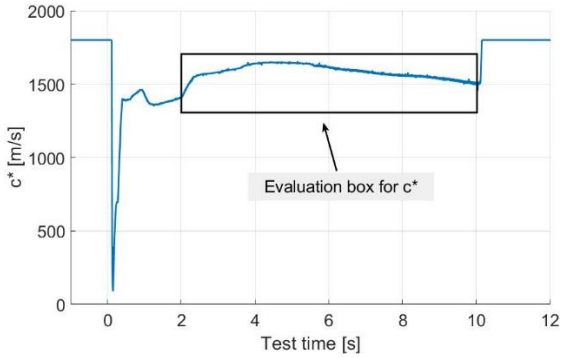

Figure 26: c evaluation during 10 s blow down test (liquid propellant ROF=6.8)*

In addition to the steady state firings, the thruster was operated in pulse mode. The different pulse lengths and t_{on}/t_{off} times are also shown in Table 4. Due to the used FCV, which was a slow-moving ball valve pressurized with nitrogen, t_{on} times below 250 ms resulted in no propellant mass flow. Thus, the shortest pulse mode with thruster operation was t_{on}=250 ms, t_{off}=750 ms.

In addition, the feeding line length in between the FCV and the thruster was approximately 0.6 m. So, depending on the propellant mass flow and density,

40-200 ms passed until the propellant entered the thruster.

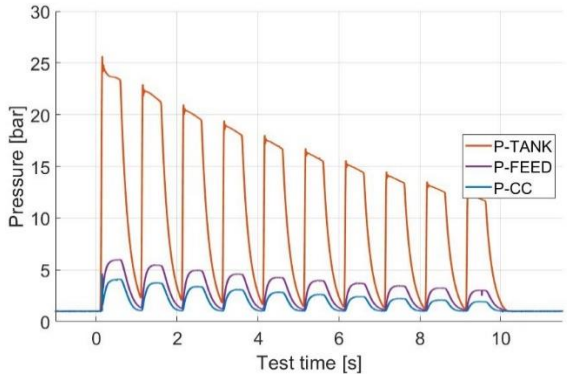

Figure 27: Pressure data during pulse mode operation, t_{on}=0.5 s t_{off}=0.5s, 10 pulses (liquid ROF=6.8)

Figure 27 shows the tank, feeding and chamber pressure during 500 ms t_{on}/500 ms t_{off} 1Hz pulse mode operation. The tank, feeding and chamber pressure show decreasing values as the pulse mode test were also conducted in blow down mode from the self-pressurizing tank. As the tank temperature drops and the liquid propellant volume reduces, the pressure in the tank also decreases. Due to the mentioned limitations of the setup (FCV inertia and line length), the rise time to 90% of the chamber pressure is approximately 200 ms. Figure 28 shows the corresponding mass flow for the shown pulse mode test. As the mass flow indicates, due to the setup volume and the valve inertia, the mass flow in between two valve openings does not drop to zero. Nevertheless, these first test show that the thruster can be operated with the HyNOx propellant in pulse mode.

The steady state and pulse mode operation resulted in a maximum temperature increase of 90°C at the chamber walls. As in between the test runs the thruster was cooled via nitrogen purge, maximum wall temperatures of 150°C were not exceeded.

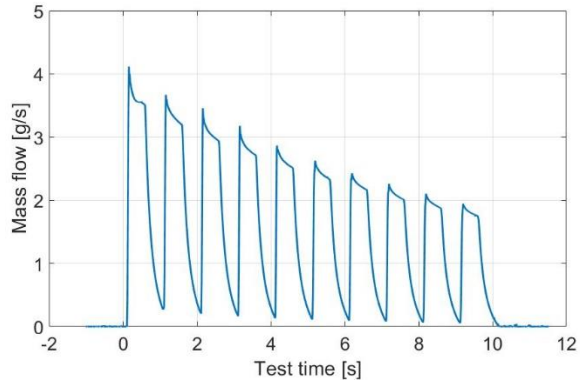

Figure 28: Pressure data during pulse mode operation, t_{on}=0.5 s t_{off}=0.5 s, 10 pulses (liquid ROF=6.8)

During the test series where a liquid propellant of ROF=6.8 was used, in between the single steady state or pulse mode firings, gas samples from the propellant tank were taken. To collect the gas samples, in between the thruster and the FVC a ball valve to close the connection to the thruster and a gas sampling port was installed (compare Figure 23).

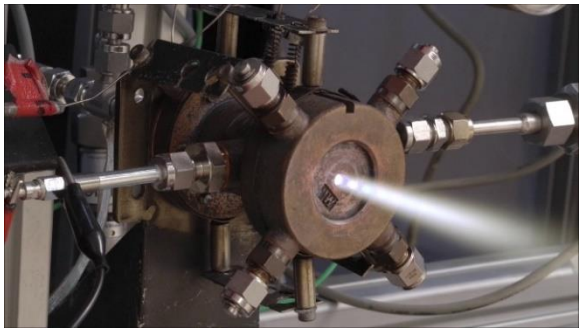

Figure 29: Experimental thruster during hot firing (liquid propellant ROF=6.8)

The results of the gas samples are shown in Table 5. The table shows the overall propellant burnt in these test series, the overall run time and the mixture ratio (ROF) of the gaseous samples as analysed via gas chromatography.

Table 5: Gas samples taken during the test run with liquid propellant ROF=6.8 and a tank filling level of 100.5 ml

Gas sample No.	Overall propellant burnt [ml]	Overall run time [s]	Gas sample ROF after test
1	53	10	9.6
2	76	15	11.2
3	88	17.5	14.3

The samples were taken consecutively after a 10 s steady state burn, then after a first and a second pulse mode operation. What Table 5 clearly indicates is that the mixture gets leaner and leaner during draining of the tank (ROF gets larger). To examine why the gaseous propellant gets leaner and leaner, the theoretical propellant data was analysed by using Refprop [39] (see Figure 30).

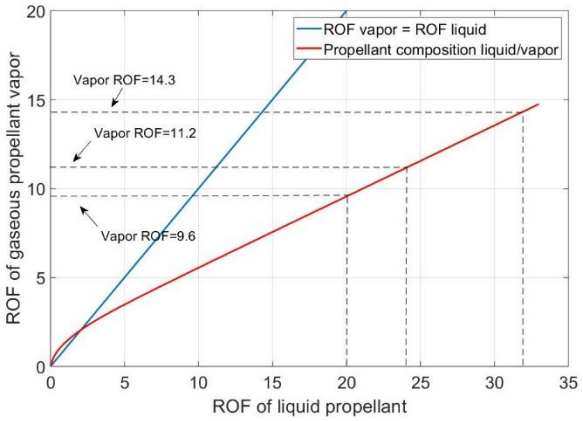

Figure 30: Composition of liquid propellant and propellant vapor for 273 K

Figure 30 shows the mixture ratio of the liquid propellant (horizontal axis) and the mixture ratio of the propellant vapor above the liquid phase (vertical axis). The red line indicates the propellants' composition for a temperature of 273 K at saturation properties. The blue line in Figure 30 indicates a (theoretic) propellant mixture, where the liquid and vapor phase have the same composition for all liquid mixture ratios. As the Refprop data of the propellant in Figure 30 show, the liquid phase is leaner than the vapor phase for mixture ratios larger than ROF=2. That means for ROF>2 the vapor phase consists of propellant with a richer mixture ratio than the liquid. So, in consequence for liquid mixture ratios larger ROF=2, the vapor phase is richer than the liquid phase. If now more and more propellant is taken from the tank in the gas phase, the remaining liquid propellant gets leaner and leaner. In relation to the liquid propellant, a larger portion of C_2H_6 evaporates and is taken from the liquid. This agrees with the gas sampling, as the sampling results in Table 5 show that the mixture gets leaner and leaner. At least these findings do not detract the usability of the propellant: as the N_2O/C_2H_6 burns up to very lean mixture ratios (theoretically up to ROF=100) the propellant in the tank could be used nearly completely. Furthermore, the results of Table 5 and *Figure 30* explain the slight decay of the c* values in *Figure 26* – as the mixture ratio gets larger with advancing test time, the theoretical and experimental c* is reduced [38].

Table 6 gives the average c* values of the experiments and the calculated combustion efficiency η_{c^*} for the steady state blow down firings. Depending on the initial liquid mixture ratio, c* values in between 1469 m/s and 1578 m/s with combustion efficiencies in between 92.1 % and 95.6% were achieved.

In sum during the atmospheric hot firings campaign 1.4 l of propellant were produced. Approximately 1.2 l of propellant were burned in the thruster during roughly 300 s of hot firing. For all tests the glow plug was a reliable ignition source and the porous injector worked flawless.

Table 6: Average c and combustion efficiency of 10 s steady state blow down tests*

Initial Liquid ROF	Average c* [m/s]	Combustion efficiency η_{c^*}
6.5	1519.7	93.7 %
9.9	1486.6	93.8 %
5.4	1469.4	92.1 %
7.7	1526.8	95.0 %
6.8	1578.2	95.6 %

6. Summary

In the frame of the ESA activity "High Performance Propellant Development" a premixed propellant consisting of N_2O and C_2H_6 was extensively studied. The propellant offers a theoretical I_{sp} above 300 s, consists of non-toxic, green components and is available at low cost. Furthermore, self-pressurized propulsion systems are realizable. Challenges of the propellant mixture are the hazards of unwanted ignition and corresponding explosion of the premixed monopropellant. In addition, high combustion temperatures have to be addressed.

In the frame of the activity the propellant's sensitivity and its behaviour in experimental propulsion systems was investigated. The following tasks were performed:

6.1. Theoretical assessment of the propellant properties

In a first work package, the theoretical propellant properties were assessed. First the propellant is non-toxic and non-carcinogenic. The highest specific impulse of approximately 300 s (10 bar chamber pressure, expansion ratio = 50) is achieved for a mixture ratio of ROF=7. A big advantage of the propellant is the possibility to allow self-pressurized propulsion systems due to its high vapor pressures. According to Refprop calculations, the density of the propellant is 728 kg/m^3 at 273 K and 39 bar.

As approximate of the TNT equivalent for gaseous deflagrations, as well as gaseous detonations, the enthalpy of combustion ΔH_C of a gaseous N_2O/C_2H_6 mixture for a constant-volume combustion was calculated and divided by enthalpy of combustion ΔH_C of 2,4,6-trinitrotoluene. Here TNT equivalent values between 0.28 and 0.31 for a mixture of ROF=7 at 300 K and a pressure of 1

to 60 atm were obtained. The TNT equivalent calculated by using CJ-detonation velocities was 0.43 with a CJ detonation velocity of 2300 m/s (Mach 8.4).

6.2. Material compatibility of the propellant

In a specific setup, the material compatibility of the N_2O/C2H6 propellant with the metallic materials Ti-6Al-4V, SS316, CRES 15-5 PH and AA2219-T85 as well as the polymers PTFE, FEP and Kalrez® 1050 LF was assessed. During the accelerated tests all four metals showed compatibility with the propellant mixture. No degradation or change in material properties was visible. Regarding the polymers, FEP is not compatible, and PTFE and Kalrez® are slightly affected in terms of their mechanical properties, although their shapes were not changed due to the immersion in the propellant.

6.3. Miscibility of the propellant

In DLR internal projects prior to the start of the described activity, a liquefaction and mixing setup was built. This setup was modified and optimised several times until a reproducible, liquid propellant mixture was obtained. The propellant was produced in different mixture ratios and the composition was assessed via gas chromatography. For at least 68 h the propellant remained in liquid, premixed state and did not show any demixing during several propellant sampling processes. Additionally, during all tests no phase separation in between the two propellant components was visible, Thus, it is assumed that the N_2O/C_2H_6 mixture forms a stable solution.

6.4. Thermal stability of the N_2O/C_2H_6 mixture

In addition to the miscibility investigations, the thermal stability of the propellant was assessed. The thermal stability test setup was connected to the miscibility setup and fed with liquid propellant mixture. By using a temperature-controlled bath, the propellant mixture was heated up to 75°C and the temperature was maintained for 45 h. The heating of the propellant resulted in pressures of up to 138 bar. During the heating period no additional pressure increase due to propellant decomposition was observed. After 48 h the propellant mixture was cooled down to ambient temperatures and gas samples of the propellant were taken. The gas analysis of the samples also did not show any decomposition of the propellant mixture. Thus, the propellant is thermally stable under the investigated conditions.

6.5. Sensitivity to adiabatic compression

To test the premixed propellant's sensitivity to adiabatic compression, a specific priming test setup was built. The setup was pretested with water to generate reference data. When tested with HyNOx propellant, the pressure peaks previously observed with water did not occur. The different behaviour in between water and the N_2O/C_2H_6 propellant is most likely caused by an instant evaporation of the propellant when the fast opening valve opens. The maximum pressure is damped by the evaporating liquid propellant and leads to a pressure gradient instead of a sharp pressure peak. All priming experiments conducted did not result in pressure peaks with the HyNOx propellant. Moreover, no self-ignition or evidence of a decomposition of the propellant was observed. Therefore, HyNOx is regarded safe in terms of adiabatic compression at the priming operation.

6.6. Hot firing thruster test under vacuum and atmospheric conditions

Hot firing tests with premixed N_2O/C_2H_6 propellant were conducted under vacuum and atmospheric conditions. For both test series an experimental 22 N thruster was used. The vacuum tests showed the propellant's ignitability under vacuum conditions. The mixture showed a good ignitability for mixture ratios (ROF) larger 5 and pressure levels in the thruster above 1.4 bar. For mixture ratios below 5 a rough combustion or a flame extinction in the thruster was observed. In sum 33 vacuum ignition tests were performed.

For the atmospheric tests, a run tank was filled with liquid propellant mixture and the thruster was fed from the gas phase above the liquid propellant mixture. With this setup the self-pressurization of the propulsion system was simulated. The tests showed a reliable ignition of the gaseous, premixed propellant via glow plug and a safe operation of the flame arrester/porous material. Furthermore, the propellant showed average c* values up to 1578 m/s and combustion efficiencies in between 92.1 and 95.6 %. Due to the gaseous, premixed state of the propellant, a very smooth combustion was achieved with a combustion roughness below 2% of the chamber pressure. Gas sampling during the test series showed that the evaporating propellant mixture gets leaner and leaner as less oxidizer is present in the gas phase than in the liquid phase. As the N_2O/C_2H_6 mixture also burns under very lean conditions, it was possible to operate the thruster until very low tank pressure levels down to nearly 1 bar. As consequence the propellant in the tank can almost completely be burnt in the thruster.

As concluding remark from the authors: despite the overall positive results of the whole activity, the propellant should always be handled with great care. As it is a highly energetic material, all

propellant related handling steps should be done with extensive safety precautions. During the investigations summarized in this paper, the premixed liquid propellant was always contained behind blast shields, protective glass or handled under remote control. Until the sensitivity of the HyNOx propellant is not studied in even greater detail, these safety precautions are strongly recommended.

7. Future development needs and outlook

The promising results of the described activities provide a solid foundation for further developments regarding premixed, green HyNOx propellants. Follow on activities should focus on two aspects: the propellant itself and the corresponding propulsion hardware.

Regarding the propellant, the specific fluid properties should be investigated in detail, e.g. the ignition temperature, the sensitivity to electrostatic discharge, the vapor pressure depending on mixture ratio and the evaporation process should be investigated and modelled. Regarding the thruster and propulsion system, first the redundancy and operation limits of the porous flame arresters should be investigated in detail. Furthermore, a regenerative cooling system should be developed as well as suitable tanks, valves and propulsion system hardware should be found, tested and finally qualified.

To assure an efficient development, further activities should be performed in close cooperation between ESA and industry.

References

[1] R.L. Sackheim, R.K. Masse, Green Propulsion Advancement: Challenging the Maturity of Monopropellant Hydrazine, Journal of Propulsion and Power 30 (2014) 265–276. https://doi.org/10.2514/1.b35086.

[2] J.D. Clark, Ignition! An informal history of liquid rocket propellants, Rutgers University Press; UMI Books on Demand, New Brunswick, N.J, Ann Abor, Mich., 2017.

[3] G.P. Sutton, O. Biblarz, Rocket propulsion elements, eighth., John Wiley & Sons; Wiley, Hoboken, N.J, 2010.

[4] Hydrazine REACH Authorisation Task Force of the European Space Industry, Position Paper; Exemption of propellant-related use of hydrazine from REACH authorisation requirement, 2012.

[5] Pierre Lionnet, Revised Space Industry Position 2020: Exemption of Propellant-related use of Hydrazine and other liquid Propellants from the Reach Authorisation Requirement, 2020. https://eurospace.org/wp-content/uploads/2020/04/hydrazine-revised-reach-position-2020-final.pdf (accessed 29 April 2020).

[6] A.S. Gohardani, J. Stanojev, A. Demairé, K. Anflo, M. Persson, N. Wingborg, C. Nilsson, Green space propulsion: Opportunities and prospects, Progress in Aerospace Sciences 71 (2014) 128–149. https://doi.org/10.1016/j.paerosci.2014.08.001.

[7] M. Persson, K. Anflo, P. Friedhoff, Flight Heritage of Ammonium Dinitramide (ADN) Based High Performance Green Propulsion (HPGP) Systems, Prop., Explos., Pyrotech. 44 (2019) 1073–1079. https://doi.org/10.1002/prep.201900248.

[8] M. Negri, M. Wilhelm, C. Hendrich, N. Wingborg, L. Gediminas, L. Adelöw, C. Maleix, P. Chabernaud, R. Brahmi, R. Beauchet, Y. Batonneau, C. Kappenstein, R.-J. Koopmans, S. Schuh, T. Bartok, C. Scharlemann, U. Gotzig, M. Schwentenwein, New technologies for ammonium dinitramide based monopropellant thrusters – The project RHEFORM, Acta Astronautica 143 (2018) 105–117. https://doi.org/10.1016/j.actaastro.2017.11.016.

[9] F. Lauck, M. Negri, M. Wilhelm, D. Freudenmann, S. Schlechtriem, M. Wurdak, U. Gotzig, Test bench preparation and hot firing tests of a 1N hydrogen peroxide monpropellant thruster, in: Space Propulsion Conference 14.-18.05.2018, Sevilla, Spain.

[10] M. Ventura, P. Mullens, The use of hydrogen peroxide for propulsion and power, in: 35th Joint Propulsion Conference and Exhibit, Los Angeles, CA, USA.

[11] M. Ventura, E.J. Wernimont, S. Heister, S. Yuan, Rocket Grade Hydrogen Peroxide (RGHP) for use in Propulsion and Power Devices - Historical Discussion of Hazards, in: 47th AIAA/ ASME/ SAE/ ASEE Joint Propulsion Conference, 31. July - 03. August 2011, San Diego, California, USA.

[12] E.J. Wernimont, System Trade Parameter Comparison of Monopropellants: Hydrogen Peroxide vs Hydrazine and Others, in: 42nd AIAA/ASME/SAE/ASEE Joint Propulsion Conference & Exhibit, 9.-12. July 2006, Sacramento, California, USA.

[13] R. Amrousse, T. Katsumi, N. Azuma, K. Hori, Hydroxylammonium nitrate (HAN)-based green propellant as alternative energy resource for potential hydrazine substitution:

From lab scale to pilot plant scale-up, Combustion and Flame 176 (2017) 334–348. https://doi.org/10.1016/j.combustflame.2016.11.011.

[14] T. Katsumi, T. Inoue, J. Nakatsuka, K. Hasegawa, K. Kobayashi, S. Sawai, K. Hori, HAN-based green propellant, application, and its combustion mechanism, Combust Explos Shock Waves 48 (2012) 536–543. https://doi.org/10.1134/S001050821205005X.

[15] R.K. Masse, R. Spores, M. Allen, AF-M315E Advanced Green Propulsion – GPIM and Beyond, in: AIAA Propulsion and Energy 2020 Forum, VIRTUAL EVENT, American Institute of Aeronautics and Astronautics, Reston, Virginia, 08242020.

[16] F. Lauck, J. Balkenhohl, M. Negri, D. Freudenmann, S. Schlechtriem, Green bipropellant development – A study on the hypergolicity of imidazole thiocyanate ionic liquids with hydrogen peroxide in an automated drop test setup, Combustion and Flame 226 (2021) 87–97. https://doi.org/10.1016/j.combustflame.2020.11.033.

[17] M. Negri, F. Lauck, Hot Firing Tests of a Novel Green Hypergolic Propellant in a Thruster, Journal of Propulsion and Power (2022) 1–11. https://doi.org/10.2514/1.B38413.

[18] H. Kang, S. Kwon, Development of 500 N Scale Green Hypergolic Bipropellant Thruster using Hydrogen Peroxide as an Oxidizer, in: 51st AIAA/SAE/ASEE Joint Propulsion Conference, 27.-29. July 2015, Orlando, Florida, USA, Orlando, FL, 2015.

[19] S.C. Ricker, D. Freudenmann, S. Schlechtriem, The Impact of Cation Structures on Hypergolicity of Thiocyanate Ionic Liquids with Hydrogen Peroxide, Energy Fuels 35 (2021) 16128–16133. https://doi.org/10.1021/acs.energyfuels.1c02427.

[20] B. Melof, M. Grubelich, Investigation of hypergolic fuels with hydrogen peroxide, in: 37th Joint Propulsion Conference and Exhibit, Salt Lake City,UT,U.S.A, American Institute of Aeronautics and Astronautics, Reston, Virigina, 2001.

[21] G. Rarata, W. Florczuk, Novel Liquid Compounds as hypergolic propellants with HTP, Journal of KONES. Powertrain and Transport 23 (2016) 271–278. https://doi.org/10.5604/12314005.1213587.

[22] J. Phillip, S. Youngblood, M.C. Grubelich, W.V. Saul, M.J. Hargather, Development and testing of a nitrous-oxide/ethanol bi-propellant rocket engine, in: 52nd AIAA/SAE/ASEE Joint Propulsion Conference, Salt Lake City, UT, American Institute of Aeronautics and Astronautics, Reston, Virginia, 2016.

[23] M. Gregory, M. Vozoff, B. Rishikof, NOFBX: A new-nontoxic Green propulsion technology with high performance and low cost, in: 63rd International Astronautical Congress, 1-5 October 2012, Naples, Italy, 2012.

[24] G. Mungas, NOFBX™ Propulsion Overview: Propulsion Challenges for Commercial Reusable Space Vehicles, in: 49th AIAA/ASME/ SAE/ ASEE Joint Propulsion Conference, 15. - 17. July, 2013, San Jose, California, USA, San Jose, CA, American Institute of Aeronautics and Astronautics, Reston, Virginia, 2013.

[25] I. Waugh, E. Moore, J. Macfarlane, A. Watts, A.E. Mayer, Testing of a novel nitrous-oxide and ethanol fuel blend, in: Space Propulsion Conference 14.-18.05.2018, Sevilla, Spain.

[26] M. Gruss, DARPA Scraps Plan To Launch Small Sats from F-15 Fighter Jet, 2015. http://spacenews.com/darpa-airborne-launcher-effort-falters/ (accessed 15 February 2018).

[27] T. Master, Airborne Launch Assist Space Access (ALASA). https://www.darpa.mil/program/airborne-launch-assist-space-access (accessed Abgerufen am: 9 February 2018).

[28] A.E. Mayer, W. Wieling, A. Watts, M. Poucet, I. Waugh, J. Macfarlane, F. Valencia-Bel, European Fuel Blend development for in-space propulsion, in: Space Propulsion Conference 14.-18.05.2018, Sevilla, Spain.

[29] A.E. Mayer, I. Waugh, M. Poucet, European Fuel Blend, Final Report: ESTEC Contract Number 4000113544/15/NL/AD, 2018.

[30] T. Pregger, G. Schiller, F. Cebulla, R.-U. Dietrich, S. Maier, A. Thess, A. Lischke, N. Monnerie, C. Sattler, P. Le Clercq, B. Rauch, M. Köhler, M. Severin, P. Kutne, C. Voigt, H. Schlager, S. Ehrenberger, M. Feinauer, L. Werling, V.P. Zhukov, C. Kirchberger, H.K. Ciezki, F. Linke, T. Methling, U. Riedel, M. Aigner, Future Fuels—Analyses of the Future Prospects of Renewable Synthetic Fuels, Energies 13 (2020) 138. https://doi.org/10.3390/en13010138.

[31] L. Werling, T. Hörger, Experimental analysis of the heat fluxes during combustion of a N 2 O/C 2 H 4 premixed green propellant in a research rocket combustor, Acta Astronautica 189 (2021) 437–451. https://doi.org/10.1016/j.actaastro.2021.07.011.

[32] L. Werling, P. Bätz, Parameters Influencing the Characteristic Exhaust Velocity of a Nitrous Oxide/Ethene Green Propellant, Journal of Propulsion and Power 38 (2022) 254–266. https://doi.org/10.2514/1.B38349.

[33] L.K. Werling, T. Hörger, K. Manassis, D. Grimmeisen, M. Wilhelm, C. Erdmann, H.K. Ciezki, S. Schlechtriem, S. Richter, T. Methling, E. Goos, C. Janzer, C. Naumann, U. Riedel, Nitrous Oxide Fuels Blends: Research on Premixed Monopropellants at the German Aerospace Center (DLR) since 2014, in: AIAA Propulsion and Energy Forum and Exposition, 2020. AIAA Propulsion and Energy Forum 24.-26.08.2020, 24.-26.08.2020.

[34] C. Naumann, T. Kick, T. Methling, M. Braun-Unkhoff, U. Riedel, ETHENE/NITROUS OXIDE MIXTURES AS GREEN PROPELLANT TO SUBSTITUTE HYDRAZINE: REACTION MECHANISM VALIDATION, Int J Energetic Materials Chem Prop 19 (2020) 65–71. https://doi.org/10.1615/IntJEnergeticMaterialsChemProp.2020028133.

[35] C. Janzer, S. Richter, C. Naumann, T. Methling, “Green propellants” as a hydrazine substitute: experimental investigations of ethane/ethene-nitrous oxide mixtures and validation of detailed reaction mechanism, CEAS Space Journal 14 (2022) 151–159. https://doi.org/10.1007/s12567-021-00370-8.

[36] Lukas Werling, Entwicklung und Erprobung von Flammensperren für einen vorgemischten, grünen Raketentreibstoff aus Lachgas (N2O) und Ethen (C2H4): DLR-Forschungsbericht. DLR-FB-2020-39, 330 S. Dissertation, Stuttgart, 2020.

[37] L. Werling, Y. Jooß, M. Wenzel, H.K. Ciezki, S. Schlechtriem, A premixed green propellant consisting of N2O and C2H4: Experimental analysis of quenching diameters to desing flashback arresters, Int J Energetic Materials Chem Prop 17 (2018) 241–262. https://doi.org/10.1615/IntJEnergeticMaterialsChemProp.2019027950.

[38] S. Gordon, B. McBride, Computer Program for Calculation of Complex Chemical Equilibrium Compositions and Applications: NASA Reference Publication 1311. I. Analysis, 1996.

[39] E. W. Lemmon, M. L. Hube, M. O. McLinden, NIST Standard Reference Database 23: Reference Fluid Thermodynamic and Transport Properties: REFPROP, Gaithersburg, 2013.

[40] EIGA EUROPEAN INDUSTRIAL GASES ASSOCIATION AISBL, SAFE PRACTICES FOR STORAGE AND HANDLING OF NITROUS OXIDE: Doc 176/19. https://www.eiga.eu/uploads/documents/DOC176.pdf (accessed 14 April 2022).

[41] B.E. Fuchs, J. Covino, E. Baker, A Critical Review of TNT Equivalency, in: International Explosives Safety Symposium & Exposition, 6-9 August 2018, San Diego CA, US.

[42] P.A. Shirbhate, M.D. Goel, A Critical Review of TNT Equivalence Factors for Various Explosives 103 471–478. https://doi.org/10.1007/978-981-15-8138-0_36.

[43] Chris Morley, Gaseq Chemcial Equilibirum Program, 2005.

[44] A. Thompson, B.N. Taylor, Guide for the Use of the International System of Units (SI): NIST Special Publication 811, 2008. https://physics.nist.gov/cuu/pdf/sp811.pdf (accessed 14 April 2022).

[45] C. Bombardieri, T. Traudt, C. Manfletti, Experimental study of water hammer pressure surge, Progress in Propulsion Physics 11 (2019) 555–570. https://doi.org/10.1051/eucass/201911555.

[46] C. Bombardieri, T. Traudt, C. Manfletti, Experimental and numerical analysis of water hammer during the filling process of pipelines, in: Space Propulsion 2014, 19.-22. Mai 2014, Cologne.

[47] United Nations, Recommendations on the transport of dangerous goods: Manual of tests and criteria, fifth., United Nations, New York, Geneva, 2009.

[48] Corvaro Francesco, Di Nicola Giovanni, Pacetti Marco, Stryjek Roman, Isochoric PVTx Measurements for the C2H6 + N2O Binary System, J. Chem. Eng. Data 51 (2006) 169–175. https://doi.org/10.1021/je0503148.

[49] O. Kunz, W. Wagner, The GERG-2008 Wide-Range Equation of State for Natural Gases and Other Mixtures: An Expansion of GERG-2004, J. Chem. Eng. Data 57 (2012) 3032–3091. https://doi.org/10.1021/je300655b.

[50] K.S. Schmitz (Ed.), Physical Chemistry: Concepts and Theory, Elsevier Science, Saint Louis, 2016.

[51] H.K. Ciezki, L. Werling, M. Negri, F. Strauss, M. Kobald, C. Kirchberger, D. Freudenmann, M. Wilhelm, A. Petrarolo, 50 Years of Test Complex M11 in Lampoldshausen - Research on Space Propulsion Systems for Tomorrow, in: 7th European Conference for Aeronautics and Space Sciences (EUCASS), 03. - 06. Jul. 2017, Milano, Italy, 2017.

[52] M. Wilhelm, L. Werling, F. Strauss, F. Lauck, C. Kirchberger, H. Ciezki, S. Schlechtriem,

Test complex M11: Research on Future Orbital Propulsion Systems and Scramjet engines, in: 70th International Astronautical Congress, Washington, USA, 2019.
[53] L. Werling, F. Lauck, D. Freudenmann, N. Röcke, H. Ciezki, S. Schlechtriem, Experimental Investigation of the Flame Propagation and Flashback Behavior of a Green Propellant Consisting of N2O and C2H4, Journal of Energy and Power Engineering 11 (2017) 735–752. https://doi.org/10.17265/1934-8975/2017.12.001.
[54] J.E. Zimmerman, B.S. Waxman, B. Cantwell, G. Zilliac, Review and Evaluation of Models for Self-Pressurizing Propellant Tank Dynamics, in: 49th AIAA/ASME/SAE/ASEE Joint Propulsion Conference 14.-17. July 2013 San Jose.
[55] G. Zilliac, M. Karabeyoglu, Modeling of Propellant Tank Pressurization, in: 41st AIAA/ASME/SAE/ASEE Joint Propulsion Conference & Exhibit 10.-13. July 2005 Tucson, Arizona.
[56] S. Borgdorff, Nitrous Oxide State Estimation in Hybrid Rocket Oxidizer Tanks. Master Thesis, Waterloo, Ontario, Canada, 2017.